IDENTIFICATION OF NOVEL BREAST CARCINOMA AND MELANOMA AVID PEPTIDES FOR IMAGING

A Thesis

presented to

the Faculty of the Graduate School

at the University of Missouri-Columbia

In Partial Fulfillment

of the Requirements for the Degree

Master of Science

---

by

XIAOFANG JIN

Dr. Thomas P. Quinn, Thesis Supervisor

JULY 2009

The undersigned, appointed by the dean of the Graduate School, have examined the thesis entitled

IDENTIFICATION OF NOVEL BREAST CARCINOMA AND MELANOMA AVID PEPTIDES FOR IMAGING

presented by Xiaofang Jin,

a candidate for the degree of [Master of Science],

and hereby certify that, in their opinion, it is worthy of acceptance.

Professor Thomas P. Quinn

Professor Susan L. Deutscher

Professor Frank J. Schmidt

Professor George P. Smith

ACKNOWLEDGEMENTS

The great experience I had as a graduate student in biochemistry department at University of Missouri will be treasured in my lifetime. I am deeply grateful for all the help and support I received. First I would take this opportunity to express my appreciation to my advisor, Dr. Thomas P. Quinn, for letting me study in his laboratory, for his guidance and cordial advice in exploring science, and especially for his encouragement when I encountered difficulties in my study and research. His patience and understanding made my graduate life successful and enjoyable.

I also want to thank my doctoral committee members, Dr. Susan L. Deutscher, Dr. Frank J. Schmidt, and Dr. George P. Smith. They have spent a great amount of their precious time on giving me critiques and inspiring suggestions on my research. From the work done in collaborated labs, Dr Deutscher lab and Dr Smith lab, I expanded my technical skills and broaden my vision in science. I would also like to say thanks to my colleges Katherine Benwell, Maura Bates, Marie Dickerson, Senthil Kumar, Jessica Newton Northup and Xiuli Zhang. It is important that they are there to help me with my experiments and life. Along with Dr. Quinn and Dr. Deutscher, we had many good times inside and outside of labs.

I would like to acknowledge other professors and graduate students in biochemistry department or life science center. They have helped me in various ways and made my graduate life colorful and complete. I will not enumerate here for the sake of the limited space.

I would like to thank the clinical biodetective training program for awarding my fellowship, which supported my research at the University of Missouri-Columbia.

I would also like to thank my beloved parents, Cuizhi Qi and Bin Jin, for whose constant encouragement and love I have received throughout my life. Thanks to my husband Ningpu Yu, for his help and encouragement in my study and life and special thanks to my little son Kevin, who actually changed my path of graduate student life.

TABLE OF CONTENTS

LIST OF ILLUSTRATIONS

Figure Page

CHAPTER 2

CHAPTER 3

LIST OF TABELS

Table Page

CHAPTER 1

CHAPTER 2

CHAPTER 3

IDENTIFICATION OF NOVEL BREAST CARCINOMA AND MELANOMA AVID PEPTIDES FOR IMAGING

Xiaofang Jin

Dr. Thomas P. Quinn, Thesis Supervisor

ABSTRACT

Development of PET (Positron Emission Tomography) and SPECT (Single Photon Emission Computed Tomography) imaging probes for melanoma and breast carcinoma are of significant importance and are in urgent need for diagnosis and treatment. Currently, FDG (fluorodeoxyglucose) is the prevailing PET probe for melanoma, while antibodies against cancer markers such as human epidermal growth factor HER2 and estradiol derivatives are used to probe breast carcinoma. However, their applications are limited either due to the low efficacy or side effects. In the past decade, several natural peptides and their derivatives were proved to be effective probes for breast carcinoma, melanoma, brain tumor, small cell lung tumor, etc.; however, they are only applicable to a certain portion of the patients with receptor positive tumors. It is hypothesized that new peptides probes specific for melanoma and breast carcinoma will be selected from peptide libraries by phage display technology. A peptide selection strategy was employed in which phage libraries were pre-cleared of peptides that bound normal vasculature and tissues in mice and peptides that bound nonmalignant human

melanocytes or breast epithelia cells. A magnetic cell sorting system was incorporated in the phage display affinity selection procedure using human melanoma TXM13 cells and breast carcinoma MD-MBA231 cells to capture tumor cells with bound phage. The selection resulted in 18 positive phage clones that were biotinylated for a cell based ELISA or conjugated with near-infrared fluorescent dye Alexa Fluor 680 for in vivo optical imaging. The selected phage were biotinylated or conjugated with a fluorescent dye at an appropriate level to avoid the negative effects of over-modification based on an optimized kinetic model for amine modification of phage coat proteins. In the cell based ELISA, two biotinylated phage clones (named M6 and M13) bound melanoma cells and one clone (M18) bound breast carcinoma cells with higher binding affinity than other phage clones and exhibited an 8-40 fold increase in signal strength compared to wild-type phage. In mice melanoma models injected with Alexa Fluor 680 conjugated phage, three phage clones (M4, M7, and M9) showed at least a two-fold increase in tumor of fluorescence postinjection compared to the pre-injection levels. Injection of 6 of the selected phage clones (M1, M2, M3, M6, M13 and M18) resulted in upregulated fluorescent signals in breast carcinoma models. Based on these data, 5 peptides (M2, M6, M7, M13 and M18) were chosen to be synthesized with an N-terminal chelator DOTA (1,4,7,10-tetraazacyclododecane-1,4,7,10-tetraacetic acid) for In-111 radiolabelling. These peptides showed reduced radioactivity absorption by up to 80% when competed by the non-radioactive In-DOTA-peptide complex on the cancer cell lines. The peptide M2 showed a preference to binding melanoma cells while the M18

peptide exhibited preference for breast carcinoma. In conclusion, the modified phage display affinity selection procedure resulted in the identification of peptides that specifically selectively targeted melanoma or breast carcinoma in vitro, two of which possessed affinity in vivo to melanoma/breast carcinoma tumors in the respective mouse model.

Chapter 1 Introduction

Melanoma

Melanoma is the most serious form of skin cancer causing 80% of deaths among patients with skin cancer, and 1.6% of deaths among all cancer patients. Its incidence rate has been steadily increasing by about 3% per year since 1981 (Cancer facts and figures 2008). There are four clinical stages for melanoma, stage I to stage IV. Generally speaking, a primary tumor is stage I, a localized tumor of greater size is stage II, the tumor metastasized to regional lymph nodes is stage III, and the tumor metastasized to distant lymph nodes or other sites in the body is stage IV. Stage I and stage II are distinguished by the thickness of the tumor. Most patients in stage I have tumors less than or equal to 1.0 mm while the size in stage II have thicker tumors that are greater than 1.0 mm. To stage melanoma, the suspected lesion area on skin is removed from the patient for biopsy. The curability of melanoma is mainly decided by the stage of the patients' disease. The survival rate at localized stage I is about 99% for a 5-year-period but only about 15% for end-stage metastatic melanoma. Furthermore, melanoma can spread to other parts of the body unpredictably and quickly, and lead to the almost incurable metastatic melanoma. Therefore, early diagnosis and disease staging are very important for improving melanoma patient survival (Cancer facts and figures 2008).

The pathogenesis of melanoma is complicated and largely unknown. The major risk factors are family history of melanoma, multiple benign or atypical

nevi, and a previous melanoma. Other factors such as immunosuppression, sun sensitivity, and exposure to ultraviolet radiation may also contribute (Miller et al., 2006). These factors associate with single genetic or a combination of mutations which alter signal pathways that control the cell survival/proliferation/ apoptosis to cause melanoma. For example, exposure to UV radiation can induce the expression of the MCR1 (melanocyte-stimulating hormone receptor) gene, a melanocyte specific receptor, responsible for pigmentation and melanogenesis (Healy, 2004; Hauser et al., 2006). The mutation and polymorphisms of MCR1 play a role in skin cancer and the over expression of MCR1 is widely found in melanoma (Siegrist et al., 1989; Rees, 2004; Han et al., 2006; Abdel-Malek et al., 2006). MCR1 stimulation leads to cyclic AMP (cAMP) production, which activates the cAMP response-element binding protein, leading to increased expression of microphthalmia transcription factor (MITF). The expressions of MITF activated the MITF pathway which is typically observed in melanoma (Miller et al., 2006).

Besides the MIFT pathway, other pathways have been identified as important in cell proliferation, adhesion, DNA damage, apoptosis and melanocyte differentiation: RAS-RAF-MEK-ERK pathway, PI3K-AKT pathway, the p16INK4A-CDK4-RB pathway, ARF-p53 pathway, the PTEN pathway, the Wnt signaling pathway and the JNK/ c-JUN pathway (Miller *et al.*, 2006). Identification of these altered pathways in melanoma has called for the need of the development of targeted imaging and therapeutic strategies, which are especially important for melanoma, since melanoma is resistant to conventional

chemotherapy (Wggermount *et al*., 2004). New agents including monoclonal antibodies, antisense oligonucleotides and tyrosine-kinase inhibitors were developed for targeted imaging and therapies in preclinical or clinical trials (Queirolo *et al*., 2006). These agents can either inhibit kinase acitivities or inhibit the receptors' function. Some of them also have the potential in cancer imaging.

Breast Carcinoma

Breast carcinoma is a very serious issue all over the world. It has the second highest mortality in cancer (after lung cancer) in women. In United States, it is estimated that there will be 182,460 new cases of invasive breast cancer and 67,770 additional cases of *in situ* breast cancer (Cancer facts and figures 2008). It is projected that 40,930 women will die from breast cancer in the U.S. in 2008. The survival rate of metastatic breast cancer is 27%, much lower than the localized disease, which is about 98%, highlighting the importance of early diagnosis and disease staging (Cancer facts and figures 2008).

Two factors very important for breast cancer diagnosis and treatment, are the hormone receptor status and human epidermal growth factor receptor 2 (HER2) gene expressions. Estrogen is a major adverse factor in human breast cancer. It is reported that the risk of breast cancer increases in young women given diethylstilbestrol to prevent abortion (Colton *et al*., 1993) and the concentrations of estradiol in breast tumors are higher than those found in the normal breast tissue (van Landeghem *et al*., 1985; Vemerulen *et al*., 1986). Moreover, high estrogen levels have been found in mouse tumor colonies and

correlated to the growth of breast tumor tissue culture (Lippman *et al*., 1976; Soule *et al*., 1980; Osbome *et al*., 1985). On molecular level, estrogen receptors can interact with several kinases, including insulin-like growth factor-1 receptor and PI3 kinase via adaptor proteins, Src and Shc, and result in different cell survival and proliferative signals via the AKT pathway and MAPK pathway (Kahlert *et al*., 2000; Levin, 2003; Simoncini *et al*., 2003; Song *et al*., 2003). Because of the role of estrogen in breast cancer, hormone therapies are used in receptor positive breast cancer, such as selective estrogen response modifiers (Tamoxifen, Toremifene) and selective estrogen receptor down-regulators (Fulvestrant) (Rugo, 2007). However, not all of the patients respond to the hormone therapies and drug resistance can develop after the initial response (Rugo, 2007).

The other important factor for breast cancer is the oncogene HER2. DNA amplification and gene over-expression of HER2 were both found in primary and metastatic breast cancer (Slamon *et al*., 1987; Berger *et al*., 1988; Parkes *et al*., 1990; Masood *et al*., 2000; Simmon *et al*., 2001). The HER2 gene is localized to chromosome 17q and encodes a transmembrane tyrosine kinase receptor protein. It can be bound and activated by growth factors and activate downstream proteins to trigger the signal cascades. The major pathways involved in HER2 activation are MAPK pathway, PI3K/Akt pathway, the JAK/ STAT pathway, and the phospholipase C (PLC) pathway (Karunagaran *et al*., 1996; Yarden *et al*., 2001). Currently, the HER2 targeted inhibitors, the monoclonal antibodies trastuzumab and pertuzumab that bind to the extracellular domain of HER2, and tyrosine

kinase inhibitors such as lapatinib that inhibit the enzymatic activity of the kinase domain, are used clinically for HER2 positive patients (Gerber, 2008). Since about 20% breast cancer patients have elevated levels of HER2 expression, these targeted therapies are not applicable to other patients and associated side effects, such as cardiac toxicity, are major concern (Gerber, 2008).

About 10-15% of patients with breast cancers are negative for estrogen receptors, progesterone receptors, and HER2 (triple-negative breast cancer). Triple-negative breast cancer is insensitive to most hormonal or targeted therapeutic agents and the major treatment is still traditional chemotherapy (Kang *et al*., 2008). New targeting agents are especially important for these breast cancer patients.

Molecular Imaging for Melanoma and Breast Carcinoma

Molecular imaging is a relatively new technology in cancer diagnosis. It is defined by Molecular Imaging Center of Excellence (MICoE) standard definitions Task Force and Society of Nuclear Medicine, "It is the visualization, characterization, and measurement of biological processes at the molecular and cellular levels in humans and other living systems." "The techniques used include radiotracer imaging/nuclear medicine, MR imaging, MR spectroscopy, optical imaging, ultrasound, and others." Positron emission tomography (PET) and single photon emission computed tomography (SPECT) are two nuclear medicine based modalities used in molecular imaging. A SPECT camera consists of a single gamma camera or multiple gamma cameras mounted on a gantry so that the

detector can record projections from many equally spaced angular intervals around the body. The most common radionuclides used in SPECT imaging are ^{99m}Tc and ^{111}In. PET must use positron-emitting radionuclides such as ^{18}F, ^{64}Cu, ^{68}Ga. In a PET camera, the paired detectors detect the annihilation photons that are produced when a positron interacts with an ordinary electron (Dale *et al.*, 2003). Fluorine-18 is the most common used positron emitting radionuclide in PET imaging; however, imaging agents that use radiometals ^{64}Cu and ^{68}Ga are currently under development. PET and SPECT have higher functional sensitivity than MRI (Magnetic Resonance Imaging) (see Table 1).

PET is an advanced technology now routinely used in oncology, mainly with the glucose analogue fluorodeoxyglucose (FDG) (Bomanji *et al.*, 2001). Cancer cells have elevated glucose consumption causing increased uptake of glucose so FDG can be used for cancer imaging (Bomanji *et al.*, 2001). It is successfully used for metastatic phase and recurrent cancer. However, because FDG has limited resolution and is unable to locate small metastatic sites PET with FDG is not useful in detecting metastasis in the stage I and II melanoma (Bomanji *et al.*, 2001). In addition, there is a significant false positive population using FDG- PET in clinical studies due to its low specificity to melanoma (Wagner *et al.*, 2005; Fink *et al.*, 2004)

For breast cancer, PET with FDG has very low sensitivity and specificity and the false negative rate is high (Hodgson *et al.*, 2008). Since estrogen receptors are up-regulated in most breast cancer patients, imaging of estrogen receptors by radiolabeled estradiol and its derivatives were used in the past (Van

de Wiele *et al*., 2000). Estrogen receptor imaging is mainly used to monitor the response of patients to the hormone therapy such as Tamoxifen. However, its application is limited to estrogen receptor positive patients. Several antibodies against other cancer markers, such as EGFR and VEGFR were developed as radiotracer for both PET and SPECT imaging (Van Dongen *et al*., 2007). For example, Anti–HER2 monoclone antibodies radiolabeled by, ^{68}Ga, ^{18}F, ^{99m}Tc, and^{111}In were applied to PET or SPECT for breast cancer. However, these agents have various side effects (Chiristian *et al*., 2007). Sigma receptors were also found to be up-regulated in breast cancer cell lines and their potential as imaging probes was investigated (Vilner *et al*., 1995). However, the first clinical report of this ligand in PET study showed a limited resolution and high possibility to cause false positive results (Caveliers *et al*., 2002).

In summary, PET with FDG has low specificity for melanoma and low sensitivity for breast carcinoma. Other targeting agents for breast carcinoma have limited resolution or various side effects and drug resistance. These issues compromise the application of PET and SPECT in these two types of cancers. Radiolabeled antibodies have high cost and various side effects, such as cardiac toxicity. New, smaller, and more selective molecular probes are needed for wide application of PET and SPECT in cancer diagnosis.

Table 1. Comparison of basic properties of MRI, PET and SPECT. The sensitive volume is the volume required to give a certain signal-to-noise ratio.

Parameter	**MRI**	**PET**	**SPECT**
Resolution	1mm	2.5mm	8mm
Sensitive Volume	10cc	0.03cc	1cc
Measured Units	nmol	nmol	nmol
Quantity Measured	Tissue Composition	Tracer Concentration	Tracer Concentration

Current Pharmaceutical Design, 2003, 9, 903-916

Peptides in Cancer Imaging

In the last decade, peptides, especially receptor binding peptides, have been applied to cancer radiology. Several tumors were found to have certain receptors over-expressed, which can be specifically bound by natural peptides with high affinity. These peptides have advantages compared to proteins and antibodies. Peptides have a smaller size and can be synthesized inexpensively, modified flexibly and radiolabeled easily. From the safety view, peptides generally have low toxicity, immunogenicity and faster body clearance (Okarvi, 1999; Blok *et al*., 1999; Boerman *et al*., 2000). The peptides developed earlier for cancer were mainly based on natural peptide hormone, such as somatostatin, gastrin, epidermal growth factor (EGF), alpha-melanocyte stimulating hormone (α-MSH), etc. (Weiner *et al*., 2005).

Radiolabeled somatostatin and its analogs were developed in late 1980s and are the most frequently used peptide for cancer imaging and peptide receptor radionuclide therapy (Krenning *et al*., 1989, 1993, 2000, Lamberts *et al*., 1991; Amold *et al*., 2000; Breeman *et al*., 2001; Riccabona *et al*., 2003; Weiner, *et al* ., 2005). Somatostatin is 14 amino acids peptide with cyclic disulphide (Ala-Gly-Cys-Lys-Asn-Phe—Phe-Trp-Lys-Thr-Phe-Thr-Ser-Cys). It can inhibit secretion of growth hormone, insulin, glucagon and gastrin and is an anti-tumor agent demonstrated on cultured tumor cells, animal models and human neuroendocrine tumor. The natural somatostatin is sensitive to enzymatic degradation and its plasma half-life is only about 3 min which compromises its in *vivo* application. Different analogs were developed to improve its plasma stability while

maintaining its physiological activity. One of the analogs octreotide (D-Phe-Cys-Phe-D-Trp-Lys-Thr-Cys-Thr) has 8 bioactive core amino acids of somatostatin and two amino acids (Phe, Trp) are replaced with D-Phe and D-Trp to extend the plasma half-life. There are five somatostatin receptors (SST 1-5) present in central nervous system, the gastrointestinal tract and some other cells of neuroendocrine origin. Octreotide showed high binding affinity to SST 2 (K_d ~2.0 nM). The DOTA or DTPA chelated octreotides radiolabeled by ^{111}In, ^{90}Y or ^{68} Ga were successfully used to image mainly neuroendocrine tumor lesions, such as carcinoid, gastrinoma, insulinoma, etc. The first report of successful melanoma imaging was performed by another analog ^{111}In-pentetreotide in a patient with a primary cutaneous melanoma and lymphatic metastases (Hoefnagel *et al*., 1994). However, in a recent clinical study of ^{111}In-DOTA-Octreotide on stage IV melanoma, the success rate to image the lesions was about half of what was reported in the original study. Moreover, in vitro study showed added SST analogs in cell culture did not inhibit growth and affect cell cycle distribution of melanoma cell lines regarding the cell populations in different growth phases (Valencak *et al*., 2005). In another study, it was shown that ^{177}Lu-octreotate did not have antitumor effects in patients with melanoma (Van Essen *et al*., 2006). So it is still unresolved whether SST analogs can be applied in treatment of melanoma.

Other peptides were developed as anti-cancer radiopharmaceuticals. α-MSH is a well characterized peptide, produced in the pituitary gland to regulate skin pigmentation (Sawyer *et al*., 1990). The α-MSH peptide binds the

melanocortin-1 receptor (MC1-R) that was reported to be upregulated in human melanoma cells (Siegrist *et al*., 1989). Natural α-MSH peptide is a linear peptide (Ac-Ser^{1}-Tyr^{2}-Ser^{3}-Met^{4}-Glu^{5}-His^{6}-Phe^{7}-Arg^{8}-Trp^{9}-Cys^{10}-Lys^{11}-Pro^{12}-Val^{13}-NH_2), with relatively low targeting efficiency, so it was modified to a cyclic peptide with nonnatural amino acids in an attempt to improve it as a specific molecular imaging agent for melanoma (Miao *et al.,* 2007). However, there are only a limited number of MCR1 receptors present on human melanoma cells (900 to 5700 per cell), which requires that the radiolabel MSH analogs must be prepared at high specific activities (Miao *et al.,* 2003). The reaction chemistry and the purification are not easily performed in the clinic, making the agent less useful than desired.

Breast cancers can express different types of peptide receptors for somatostatin, gastrin releasing peptide or bombesin (GRP) and neuropeptide (NP)-Y analogues NPY (Y1) (Reubi *et al*., 2002). A somastatin analog permits identification of breast cancer in 75% cases (Van Reijck *et al*., 1994). GRP receptors are abundant in most breast cancer cells (67%). One of bombesin analogs, ^{99m}Tc RP527, showed specific uptake in four of six breast and one of four prostate carcinomas (Giacchetti *et al*., 1990; Gugger *et al*., 1999; Van de Wiele *et al*., 2000). NPY receptors are present in breast carcinomas, adrenal gland and related tumors, renal cell carcinomas, and ovarian cancers in both tumor cells and tumor-associated blood vessels (Körner *et al*., 2007). They are present in 85% of the breast carcinomas and their in *vivo* application was still in the process of animal models (Reubi *et al*., 2001; Langer *et al*., 2001).

At present, only one peptide for melanoma and a few peptides for breast cancer are available as potential imaging agents. Their receptors are only present in some patients, so these patients with receptor negative tumors do not respond to the radiology imaging. More peptides are needed as alternative choices for patients with these receptor-negative tumors. These new peptide probes will also facilitate cancer biology research.

Phage Display for Molecular Targets in Cancer

Bacteriophage (phage) display is a well established technique that is often applied in the development of molecular probes. Exogenous peptide or protein sequences can be introduced into the genes encoding phage coat protein and thus these encoded peptides or proteins can be expressed with coat proteins on phage surfaces (Smith *et al*., 1985). Instead of getting genetically engineered peptides or proteins one by one, it is easy to generate large populations of phage, displaying millions of different inserted sequences to form random peptide or antibody libraries. Four strains of filamentous phage particles (M13, f1, Fd and ft) are commonly used for display. The surface of filamentous phage is primarily composed of pVIII protein, with the minor coat protein pIII located at one end of the particle, as well as other coat proteins. A foreign peptide or protein is fused genetically to either to 1 to 5 copies of the minor coat protein pIII, or to 1 to ~3000 copies of the major coat protein pVIII. In the library, each phage clone can express a single peptide, which can be linear or constrained sequences. Constrained libraries have two cysteine residues flanking a random length of

peptide and facilitate the formation of a disulfide bond. An affinity selection starts with a phage library or subset of the library, which is exposed to immobilized targets such as receptors, antibodies, enzymes or other binding molecules. The unbound phage are washed away and bound phage are eluted and amplified by infecting the corresponding bacteria cells. The amplified population is then used as input to next round of selection. Three or four rounds of selection are performed and the target-binding phage clones are enriched during this process. By sequencing these clones, the peptide sequences expressed on the surface of the phage can be deduced and the individual phage clones or chemically synthesized peptides can be used as molecular probes (Smith *et al*, 1985).

In the past, phage display technology has been successfully used to explore protein-protein interaction, enzyme-substrate pairs, epitope mapping and antibody engineering (Sachdev, 2005). For cancer imaging and therapeutics, phage display was used as an in *vitro* strategy to select the antibodies or antibody variable fragments that can target cancer cells and it also serves to generate recombinant antibody fragments, which greatly facilitated cancer immunotherapy (Brekke *et al*., 2003; Ben-Kasus *et al*., 2008). Anti-cancer antibodies and antibody fragments have high tumor binding activity and specificity but have a longer circulation half-life in vivo due to their high molecular weight. In contrast, peptides have a short in vivo circulation half life but a good tumor binding affinity, so phage display plays an arising role in identification and development of peptide molecular probes. For example, the integrin binding RGD motif was identified in 1996 (Arap *et al*., 1998; Pasqualini *et al*., 1996) from phage library selection.

``Phage libraries have also been selected in vivo by intravenous injection into animals, followed by collection of target organs or tissues, and elution of bound phage clones. To date, several peptides have been selected by phage display to target receptors on carcinoma cells or related to angiogenesis. For example, the eight-amino acid peptide CRFWKTWC was selected for somatostatin receptor and several peptides (MARSGL, MARAKE, MYWGDSHWLQYWYE and KCCYSL) for HER2 receptor (Houimel *et al*., 2001; Karasseva *et al*., 2002; Urbanelli *et al*., 2001). Our lab has already identified the six-amino acid peptide, KCCYSL by phage display technology to target HER2 receptor and it was found to be a new imaging candidate in a pre-clinical study for breast cancer (Kumar *et al*., 2007).

In summary, peptides are attractive as molecular probes due to their rapid in vivo pharmacokinetics and high affinities for their cognate receptors. Historically, somatostatin analogs were the first class of receptor binding peptides to gain clinical application. Other natural regulatory peptides such as VIP and bombesin are under development. Molecular imaging is a powerful tool for cancer diagnosis and monitoring but has limited roles in melanoma and breast carcinoma due to lack of appropriate imaging probes. New peptides can be identified by phage display technology, which approach has already yielded functional peptides previously.

We hypothesized that the bacteriophage (phage) display technique coupled with optical animal imaging selection is an effective method to screen for new

peptides that could bind melanoma or breast carcinoma, therefore can be used as molecular probes for cancer imaging.

REFERENCE

2007. NPY and cohorts in human disease. Proceedings of the 8th International NPY Meeting. April 22-26, 2006. St. Petersburg, Florida, USA. Peptides 28: 197-483.

Abdel-Malek ZA, et al. 2006. Melanoma prevention strategy based on using tetrapeptide alpha-MSH analogs that protect human melanocytes from UV-induced DNA damage and cytotoxicity. FASEB J 20: 1561-1563.

Arap W, Pasqualini R, Ruoslahti E. 1998. Cancer treatment by targeted drug delivery to tumor vasculature in a mouse model. Science 279: 377-380.

Arnold R, Simon B, Wied M. 2000. Treatment of neuroendocrine GEP tumors with somatostatin analogues: a review. Digestion 62 Suppl 1: 84-91.

Bailey DL, Adamson KL. 2003. Nuclear medicine: from photons to physiology. Curr Pharm Des 9: 903-916.

Ben-Kasus T, Schechter B, Sela M, Yarden Y. 2007. Cancer therapeutic antibodies come of age: Targetingminimal residual disease. Mol Oncol 1: 42-54.

Berger MS, Locher GW, Saurer S, Gullick WJ, Waterfield MD, Groner B, Hynes NE. 1988. Correlation of c-erbB-2 gene amplification and protein expression in human breast carcinoma with nodal status and nuclear grading. Cancer Res 48: 1238-1243.

Blok D, Feitsma RI, Vermeij P, Pauwels EJ. 1999. Peptide radiopharmaceuticals in nuclear medicine. Eur J Nucl Med 26: 1511-1519.

Boerman OC, Oyen WJ, Corstens FH. 2000. Radio-labeled receptor-binding peptides: a new class of radiopharmaceuticals. Semin Nucl Med 30: 195-208.

Bomanji JB, Costa DC, Ell PJ. 2001. Clinical role of positron emission tomography in oncology. Lancet Oncol 2: 157-164.

Breeman WA, de Jong M, Kwekkeboom DJ, Valkema R, Bakker WH, Kooij PP, Visser TJ, Krenning EP. 2001. Somatostatin receptor-mediated imaging and therapy: basic science, current knowledge, limitations and future perspectives. Eur J Nucl Med 28: 1421-1429.

Brekke OH, Loset GA. 2003. New technologies in therapeutic antibody development. Curr Opin Pharmacol 3: 544-550.

Caveliers V, Everaert H, John CS, Lahoutte T, Bossuyt A. 2002. Sigma receptor scintigraphy with N-[2-(1'-piperidinyl)ethyl]-3-(123)I-iodo-4-methoxybenzamide of patients with suspected primary breast cancer: first clinical results. J Nucl Med 43: 1647-1649.

Colton T, Greenberg ER, Noller K, Resseguie L, Van Bennekom C, Heeren T, Zhang Y. 1993. Breast cancer in mothers prescribed diethylstilbestrol in pregnancy. Further follow-up. JAMA 269: 2096-2100.

Eggermont AM, Kirkwood JM. 2004. Re-evaluating the role of dacarbazine in metastatic melanoma: what have we learned in 30 years? Eur J Cancer 40: 1825-1836.

Fink AM, Holle-Robatsch S, Herzog N, Mirzaei S, Rappersberger K, Lilgenau N, Jurecka W, Steiner A. 2004. Positron emission tomography is not useful in detecting metastasis in the sentinel lymph node in patients with primary malignant melanoma stage I and II. Melanoma Res 14: 141-145.

Gerber DE. 2008. Targeted therapies: a new generation of cancer treatments. Am Fam Physician 77: 311-319.

Giacchetti S, Gauville C, de Cremoux P, Bertin L, Berthon P, Abita JP, Cuttitta F, Calvo F. 1990. Characterization, in some human breast cancer cell lines, of gastrin-releasing peptide-like receptors which are absent in normal breast epithelial cells. Int J Cancer 46: 293-298.

Han J, Kraft P, Colditz GA, Wong J, Hunter DJ. 2006. Melanocortin 1 receptor variants and skin cancer risk. Int J Cancer 119: 1976-1984.

Hauser JE, Kadekaro AL, Kavanagh RJ, Wakamatsu K, Terzieva S, Schwemberger S, Babcock G, Rao MB, Ito S, Abdel-Malek ZA. 2006. Melanin content and MC1R function independently affect UVR-induced DNA damage in cultured human melanocytes. Pigment Cell Res 19: 303-314.

Healy E. 2004. Melanocortin 1 receptor variants, pigmentation, and skin cancer susceptibility. Photodermatol Photoimmunol Photomed 20: 283-288.

Hodgson NC, Gulenchyn KY. 2008. Is there a role for positron emission tomography in breast cancer staging? J Clin Oncol 26: 712-720.

Hoefnagel CA, Rankin EM, Valdes Olmos RA, Israels SP, Pavel S, Janssen AG. 1994. Sensitivity versus specificity in melanoma imaging using iodine-123 iodobenzamide and indium-111 pentetreotide. Eur J Nucl Med 21: 587-588.

Houimel M, Schneider P, Terskikh A, Mach JP. 2001. Selection of peptides and synthesis of pentameric peptabody molecules reacting specifically with ErbB-2 receptor. Int J Cancer 92: 748-755.

Kahlert S, Nuedling S, van Eickels M, Vetter H, Meyer R, Grohe C. 2000. Estrogen receptor alpha rapidly activates the IGF-1 receptor pathway. J Biol Chem 275: 18447-18453.

Kang SP, Martel M, Harris LN. 2008. Triple negative breast cancer: current understanding of biology and treatment options. Curr Opin Obstet Gynecol 20: 40-46.

Karasseva NG, Glinsky VV, Chen NX, Komatireddy R, Quinn TP. 2002. Identification and characterization of peptides that bind human ErbB-2 selected from a bacteriophage display library. J Protein Chem 21: 287-296.

Karunagaran D, Tzahar E, Beerli RR, Chen X, Graus-Porta D, Ratzkin BJ, Seger R, Hynes NE, Yarden Y. 1996. ErbB-2 is a common auxiliary subunit of NDF and EGF receptors: implications for breast cancer. EMBO J 15: 254-264.

Korner M, Reubi JC. 2007. NPY receptors in human cancer: a review of current knowledge. Peptides 28: 419-425.

Krenning EP, Bakker WH, Breeman WA, Koper JW, Kooij PP, Ausema L, Lameris JS, Reubi JC, Lamberts SW. 1989. Localisation of endocrine-related tumors with radioiodinated analogue of somatostatin. Lancet 1: 242-244.

Krenning EP, et al. 1993. Somatostatin receptor scintigraphy with [111In-DTPA-D-Phe1]- and [123I-Tyr3]-octreotide: the Rotterdam experience with more than 1000 patients. Eur J Nucl Med 20: 716-731.

Kumar R. 2007. Targeted functional imaging in breast cancer. Eur J Nucl Med Mol Imaging 34: 346-353.

Kwekkeboom D, Krenning EP, de Jong M. 2000. Peptide receptor imaging and therapy. J Nucl Med 41: 1704-1713.

Lamberts SW, Krenning EP, Reubi JC. 1991. The role of somatostatin and its analogs in the diagnosis and treatment of tumors. Endocr Rev 12: 450-482.

Langer M, La Bella R, Garcia-Garayoa E, Beck-Sickinger AG. 2001. 99mTc-labeled neuropeptide Y analogues as potential tumor imaging agents. Bioconjug Chem 12: 1028-1034.

Levin ER. 2003. Bidirectional signaling between the estrogen receptor and the epidermal growth factor receptor. Mol Endocrinol 17: 309-317.

Lippman M, Bolan G, Huff K. 1976. The effects of estrogens and antiestrogens on hormone-responsive human breast cancer in long-term tissue culture. Cancer Res 36: 4595-4601.

Masood S, Bui MM. 2000. Assessment of Her-2/neu overexpression in primary breast cancers and their metastatic lesions: an immunohistochemical study. Ann Clin Lab Sci 30: 259-265.

Miao Y, Whitener D, Feng W, Owen NK, Chen J, Quinn TP. 2003. Evaluation of the human melanoma targeting properties of radiolabeled alpha-melanocyte stimulating hormone peptide analogues. Bioconjug Chem 14: 1177-1184.

Miao Y, Benwell K, Quinn TP. 2007. 99mTc- and 111In-labeled alpha-melanocyte-stimulating hormone peptides as imaging probes for primary and pulmonary metastatic melanoma detection. J Nucl Med 48: 73-80.

Miller AJ, Mihm MC, Jr. 2006. Melanoma. N Engl J Med 355: 51-65.

Okarvi SM. 1999. Recent developments in 99Tcm-labelled peptide-based radiopharmaceuticals: an overview. Nucl Med Commun 20: 1093-1112.

Osborne CK, Hobbs K, Clark GM. 1985. Effect of estrogens and antiestrogens on growth of human breast cancer cells in athymic nude mice. Cancer Res 45: 584-590.

Parkes HC, Lillycrop K, Howell A, Craig RK. 1990. C-erbB2 mRNA expression in human breast tumors: comparison with c-erbB2 DNA amplification and correlation with prognosis. Br J Cancer 61: 39-45.

Pasqualini R, Ruoslahti E. 1996. Organ targeting in vivo using phage display peptide libraries. Nature 380: 364-366.

Queirolo P, Acquati M. 2006. Targeted therapies in melanoma. Cancer Treat Rev 32: 524-531.

Reubi JC, Gugger M, Waser B, Schaer JC. 2001. Y(1)-mediated effect of neuropeptide Y in cancer: breast carcinomas as targets. Cancer Res 61: 4636-4641.

Reubi C, Gugger M, Waser B. 2002. Co-expressed peptide receptors in breast cancer as a molecular basis for in vivo multireceptor tumour targeting. Eur J Nucl Med Mol Imaging 29: 855-862.

Riccabona G, Decristoforo C. 2003. Peptide targeted imaging of cancer. Cancer Biother Radiopharm 18: 675-687.

Rugo HS. 2007. Hormonal therapy for advanced breast cancer. Hematol Oncol Clin North Am 21: 273-291.

Sawyer TK, Staples DJ, Castrucci AM, Hadley ME, al-Obeidi FA, Cody WL, Hruby VJ. 1990. Alpha-melanocyte stimulating hormone message and inhibitory sequences: comparative structure-activity studies on melanocytes. Peptides 11: 351-357.

Siegrist W, Solca F, Stutz S, Giuffre L, Carrel S, Girard J, Eberle AN. 1989. Characterization of receptors for alpha-melanocyte-stimulating hormone on human melanoma cells. Cancer Res 49: 6352-6358.

Simon R, et al. 2001. Patterns of her-2/neu amplification and overexpression in primary and metastatic breast cancer. J Natl Cancer Inst 93: 1141-1146.

Simoncini T, Hafezi-Moghadam A, Brazil DP, Ley K, Chin WW, Liao JK. 2000. Interaction of oestrogen receptor with the regulatory subunit of phosphatidylinositol-3-OH kinase. Nature 407: 538-541.

Slamon DJ, Clark GM, Wong SG, Levin WJ, Ullrich A, McGuire WL. 1987. Human breast cancer: correlation of relapse and survival with amplification of the HER-2/neu oncogene. Science 235: 177-182.

Smith GP. 1985. Filamentous fusion phage: novel expression vectors that display cloned antigens on the virion surface. Science 228: 1315-1317.

Song RX, McPherson RA, Adam L, Bao Y, Shupnik M, Kumar R, Santen RJ. 2002. Linkage of rapid estrogen action to MAPK activation by ERalpha-Shc association and Shc pathway activation. Mol Endocrinol 16: 116-127.

Soule HD, McGrath CM. 1980. Estrogen responsive proliferation of clonal human breast carcinoma cells in athymic mice. Cancer Lett 10: 177-189.

Urbanelli L, Ronchini C, Fontana L, Menard S, Orlandi R, Monaci P. 2001. Targeted gene transduction of mammalian cells expressing the HER2/neu receptor by filamentous phage. J Mol Biol 313: 965-976.

Valencak J, Heere-Ress E, Traub-Weidinger T, Raderer M, Schneeberger A, Thalhammer T, Aust S, Hamilton G, Virgolini I, Pehamberger H. 2005. Somatostatin receptor scintigraphy with 111In-DOTA-lanreotide and 111In-DOTA-Tyr3-octreotide in patients with stage IV melanoma: in-vitro and in-vivo results. Melanoma Res 15: 523-529.

Van de Wiele C, De Vos F, Slegers G, Van Belle S, Dierckx RA. 2000. Radiolabeled estradiol derivatives to predict response to hormonal treatment in breast cancer: a review. Eur J Nucl Med 27: 1421-1433.

Van de Wiele C, Dumont F, Vanden Broecke R, Oosterlinck W, Cocquyt V, Serreyn R, Peers S, Thornback J, Slegers G, Dierckx RA. 2000. Technetium-99m RP527, a GRP analogue for visualisation of GRP receptor-expressing malignancies: a feasibility study. Eur J Nucl Med 27: 1694-1699.

van Dongen GA, Visser GW, Lub-de Hooge MN, de Vries EG, Perk LR. 2007. Immuno-PET: a navigator in monoclonal antibody development and applications. Oncologist 12: 1379-1389.

van Essen M, Krenning EP, Kooij PP, Bakker WH, Feelders RA, de Herder WW, Wolbers JG, Kwekkeboom DJ. 2006. Effects of therapy with [177Lu-DOTA0, Tyr3]octreotate in patients with paraganglioma, meningioma, small cell lung carcinoma, and melanoma. J Nucl Med 47: 1599-1606.

van Landeghem AA, Poortman J, Nabuurs M, Thijssen JH. 1985. Endogenous concentration and subcellular distribution of estrogens in normal and malignant human breast tissue. Cancer Res 45: 2900-2906.

Vermeulen A, Deslypere JP, Paridaens R, Leclercq G, Roy F, Heuson JC. 1986. Aromatase, 17 beta-hydroxysteroid dehydrogenase and intratissular sex hormone concentrations in cancerous and normal glandular breast tissue in postmenopausal women. Eur J Cancer Clin Oncol 22: 515-525.

Vilner BJ, John CS, Bowen WD. 1995. Sigma-1 and sigma-2 receptors are expressed in a wide variety of human and rodent tumor cell lines. Cancer Res 55: 408-413.

Wagner JD, Schauwecker D, Davidson D, Logan T, Coleman JJ, 3rd, Hutchins G, Love C, Wenck S, Daggy J. 2005. Inefficacy of F-18 fluorodeoxy-D-glucose-positron emission tomography scans for initial evaluation in early-stage cutaneous melanoma. Cancer 104: 570-579.

Weiner RE, Thakur ML. 2005. Radiolabeled peptides in oncology: role in diagnosis and treatment. BioDrugs 19: 145-163.

Widakowich C, de Castro G, Jr., de Azambuja E, Dinh P, Awada A. 2007. Review: side effects of approved molecular targeted therapies in solid cancers. Oncologist 12: 1443-1455.

Yarden Y, Sliwkowski MX. 2001. Untangling the ErbB signalling network. Nat Rev Mol Cell Biol 2: 127-137.

Chapter 2 Identification of Novel Peptides by Phage Display Potentially as Cancer Imaging Agents

INTRODUTION

Melanoma and breast carcinoma are two serious issues in public health. There were 62,480 new cases of melanoma in the US in 2008 and the incidence of melanoma has been increasing by about 3% per year since 1981. Melanoma spreads to other parts of the body unpredictably and quickly, which leads to almost incurable metastatic disease. Breast cancer has the second highest malignancy mortality (after lung cancer) in women. It is estimated that there will be 182,460 new cases of invasive breast cancer and 67,770 additional cases of *in situ* breast cancer in US in 2008. The survival rates of both cancers are much higher in early stage than in the late stage, which highlights the importance of early diagnosis (Cancer facts and figures 2008).

Cancer imaging is critical in diagnosis and treatment of patients. PET (Positron Emission Tomography) and SPECT (Single Photon Emission Computed Tomography) are two widely used modalities in cancer imaging due to their functional sensitivity compared to other modalities such as MRI (Magnetic Resonance Imaging), ultrasound, X-ray, etc. (Bailey, *et al*, 2003). In PET and SPECT imaging, a patient is given an injection of radiolabeled cancer homing

agent, which can help localize tumors because the tumor cells have higher radiotracer uptake than normal cells in the body. The distribution of the radiolabeled cancer targeting agent in the patient is collected by PET or SPECT scans, and later converted to a 3D medical image. Currently, FDG (fluorodeoxyglucose) is the prevailing agent used in PET for visualizing melanoma (Bomanji *et al*., 2001), while molecular imaging approaches involving antibodies against cancer markers and estradiol derivatives are used to target breast carcinoma (Van de Wiele *et al*., 2000; Van Dongen *et al*., 2007). However, ^{18}F-FDG is not able to detect reproducibly melanoma metastases (Wagner *et al*., 2005; Fink *et al*., 2004) and phase I and II of breast carcinoma (Hodgson *et al*., 2008). The application of ^{18}F-FDG is limited to patients who have up-regulated glucose metabolism level in their tumors. Furthermore, side effects of some antibodies and estradiol derivatives are of concern during diagnosis (Widakowich, *et al*., 2007).

During the past decade, peptides have emerged as imaging probes due to high target specificity, low toxicity and rapid pharmacokinetics. Although they have proven to be effective targeting agents on several types of cancer, only a few natural peptides and their derivatives are available for clinical use now (Okarvi, 1999; Blok *et al*., 1999; Boerman *et al*., 2000). It is urgent and important to identify new peptides for cancer diagnosis, detection and impact treatment management.

Bacteriophage (phage) display is a well established technique applied to select anti-cancer peptides, such as peptides that bound to somatostatin receptor,

HER2 receptor, Thomsen-Friedenreich antigen, kinase, etc. (Landon *et al*., 2004). Phage particles can tolerate the introduction of exogenous sequences encoding 6-45 amino acids into the genes of phage coat proteins and thus these encoded peptides can be expressed as fused proteins to the native coat proteins on phage surfaces (Smith *et al*., 1985). In an affinity selection, a peptide library is exposed to immobilized targets such as receptor, antibody, enzyme or other binding molecules. The unbound phage are washed away and bound phage are eluted and amplified by infecting the corresponding bacteria cells. The amplified eluate is then used as input to the next round of selection. Three or four rounds of selection are typically performed enriching the phage population for viron particles that display peptide that bound the target molecules (Smith *et al.*, 1985). Two important factors are used to monitor the affinity selection: the yield and enrichment factor. Yield is the fraction of particles that survive the selection. It can be calculated as follows: Yield= (total number of output TUs)/(total number of input TUs). During the selection, the fd-cat virons display no foreign peptides, therefore they can serve as an internal indicator of non-specific background yield during affinity selection. The fd-cat virons are mixed with the input phage, and the enrichment factor can be calculated as follows: Enrichment= (percent yield of library phage)/(percent yield of control phage).

Here we applied this peptide phage display to select new peptides that can bind specifically to melanoma or breast carcinoma as potential probes for molecular imaging. The peptide libraries were administrated in mouse circulation system and incubated with normal human cell lines prior to the cancer cell line

affinity selection in order to lower the background binding. The winners from the selection were tested for their binding capacities to melanoma and breast carcinoma cell lines and an in *vivo* animal fluorescence assay was also designed to provide additional in *vivo* properties of phage clones. A few peptides were identified to be potential imaging probes.

MATERIALS AND METHODS

All phage libraries and manipulations including propagation, sequencing, purification, quantification and sequencing were conducted according to protocols by Dr. George Smith. (Smith GP, 1985; 2006)

Cell Lines and Culture

Human epidermal melanocytes (HEM) (Catalog Number: 2200/2210/2220) were purchased from ScienCell™ Research Laboratories, Inc (Carlsbad, CA).The melanocytes were cultured following the instruction provided by ScienCell™ Research Laboratories, Inc. Human breast epithelial cells 184A1 (Catalog Number: CRL-8789) were purchased from American Type Tissue Culture Collection (ATCC) (Manassas, Virginia). The 184A1 cells were cultured following the instruction provided from ATCC. Human melanoma cells TXM13 were supplied by Dr. Janet Price of the Cell Biology Department, University of Texas M. D. Anderson Cancer Center. The human breast carcinoma cell line MDA-MB-231(Catalog Number: HTB-26™) was purchased from ATCC. These two cancer cell lines were cultured in RPMI 1640 (Invitrogen, Carlsbad, CA) containing 10% heat-inactivated FCS and 48 mg/L of gentamicin (Invitrogen). The cells were cultured in tissue culture flasks and kept in a humidified atmosphere of 5% CO_2 at 37°C. The cells were detached from the flasks by cell dissociation buffer (Invitrogen) for subculture.

Depletions of the Mouse Pre-cleared Phage Libraries

Three phage libraries, f3-15mer, f88-15mer and f88-Cys6 were provided by Dr. George Smith (University of Missouri-Columbia, Columbia, MO). The f88 phage has foreign peptides fused with coat protein pVIII, and the f3 fused with coat protein pIII. The designation "15mer" refers to the expressed random peptides that are of 15 amino acids length while "cys6" denotes two cystines flanking 6 random amino acids. The f3-15mer, f88-15mer and f88-Cys6 phage libraries were injected into SCID mice and recovered from the blood to form the mouse pre-cleared libraries.

The pre-cleared phage libraries were prepared (in 2007) and the amplified output were used as our initial libraries. Briefly, the SCID female mice were injected intravenously with 200 µl f88-15mer library (1.144×10^{14} virions/ml; 2×10^{9} primary clones, infectivity 25.5%), or 200 µl f88-Cys6 library (1.87×10^{14} virions/ml; 2.7×10^{8} primary clones, infectivity 10.01%), or with 200 µl f3-15mer (fUSE5/15-mer) library (2.5×10^{8} primary clones; 1.74×10^{14} virions/ml, infectivity 12.6%),). After 15 min, each mouse was bled by cardiac puncture into a syringe containing 2 mM EDTA in D-PBS without Mg or Ca and the bloods were pooled in a single 15-ml screw-cap tube and diluted to 8 ml with CMF. The phage clones were precipitated and amplified as mouse pre-cleared libraries. The representation of the three libraries f88-15mer, f88-Cys6 and f3-15mer are 41.6, 362, 22.6 infected cells per primary clones.

In the positive screen method, the phage were exposed to three reagents: anti-melanoma MACS magnetic beads (Catalog #130-090-452); LD columns (Catalog #130-042-901) and anti-ErbB2 MACS magnetic beads (Catalog #130-

090-482). To remove the phage that bind to these three components, the three mouse pre-cleared libraries f3-15mer, f88-15mer and f88-Cys6 consisting 1.8×10^{14}, 0.9×10^{14} and 1×10^{14} clones, were incubated with 300µl anti-melanoma MACS magnetic beads or anti-ErbB2 MACS magnetic beads from the 2ml vendor's stock for 16 hr at 4°C. Then the mixtures were passed through the LD column in the QuadroMACS separator (Milteny Biotec Inc.), washed with 2 ml degassed running buffer (Dulbecco's PBS without calcium and magnesium, Invitrogen). The effluents were collected and pipetted into the column again and then washed with another 3ml running buffer. The final effluents were collected and phage were precipitated and amplified as the column/bead-depleted libraries.

The column/bead-depleted libraries were added into T-150 flasks with HEM melanocytes or 184A1 breast epithelial cells ~90% confluent at 37º for 4 hours. Unbound phage in the medium were collected and amplified. These libraries were ready for the positive screen.

Positive Screen on Human Cancer Cell Lines

The magnetic cell sorting system (MACS) (purchased from Milteny Biotec Inc., Auburn, CA) was combined with phage display affinity selection in the positive screen. Anti-melanoma MACS magnetic beads (Catalog #130-090-452), anti-ErbB2 MACS magnetic beads (Catalog #130-090-482) and other MACS supplies were purchase from Milteny Biotec. The positive screen was performed by MACS following the instruction from Milteny Biotec. Approximate 2×10^7 TXM13 or MDA-MB-231 cells were mixed with 100µl FcR Blocking

Reagent (Catalog #130-059-901) and 100 μl of the corresponding MACS beads and incubated for 30 minutes at 4°C. The mixture was diluted by 10 ml running buffer (Dulbecco's PBS without calcium and magnesium, Invitrogen) and centrifuged at 300×g for 10 minutes. The cell pellets were resuspended in 40 ml RPMI 1640 and the depleted libraries consisting 6.2×10^{12} virons were added respectively. After 4h incubation at room temperature, they were loaded to LS columns (Catalog #130-042-401) in the QuadroMACS separator (Milteny Biotec Inc.) and washed by 30 ml PBS (Invitrogen). Cells were released from the column by removing from the separator and lysed by 2.5% CHAPS (Invitrogen) in TBS (150 mM NaCl, 50 mM Tris, pH adjusted to 7.5 with HCl). After centrifuge 8,000g for 30 min, phage in the supernatant were collected, titered and amplified, and a portion was used for next round of selection. After four rounds of selection, the phage were plated and single clones were randomly selected and sequenced. The amino acid sequences of inserted peptides were deduced from the DNA sequences.

Conjugation of Biotin and AF 680 Phage Particles

Biotinylating reagent NHS-PEO_4-biotin (Catalog number 21329, Pierce Chemical Co., Rockford, IL), and the NIR fluorophor labeling reagent sulfo-NHS-AF680 (Catalog number A20008, Invitrogen) were dissolved in dimethylsulfoxide (DMSO) immediately prior to usage. Phage virions were diluted in CMF (136.9 mM NaCl, 2.68 mM KCl, 8.1 mM Na_2HPO_4, and 1.47 mM KH_2PO_4, pH 7.2). For the reaction, 0.1M NaH_2PO_4 was added first. Then phage

and reagents were added and vortexed immediately for a few minutes. The reactions were allowed to continue overnight (~12–18 hr) at room temperature in the dark. In the reaction, 5.0×10^{13} virons/ml of phage virons were mixed with 6.4 mM NHS-PEO_4-biotin, and 7×10^{12} virons/ml were mixed with 194 μM sulfo-NHS-AF680.

Cell Based Enzyme-linked Immunosorbant Assay

HEM, 184 A1, TXM13 or MDA-MB-231 cells were grown to 90% confluency in tissue culture–treated 96-well plates (Costar, Cambridge, MA). The growth mediums were removed, and various biotinylated phage concentration (1×10^9 to 1×10^{12} virons/ml) in binding medium (RPMI 1640 plus 10%FBS) were added to the plates. The plate was incubated at 37°C for 1 hr then washed with binding medium three times followed by seven times with washing buffer (1mM $CaCl_2$, 0.5mM $CaCl_2$, 1%BSA in TBS). Wells were reacted for 30 min at room temperature with 100 μl AP-SA (Catalog number 016-050-084, Jackson ImmunoResearch, West Grove, PA) at 200 ng/ml in TBS/Tween (TBS supplemented with 0.5% Tween 20) and washed. 100μl NPP buffer (1M diethanolamine buffer pH 9.8, 1 mM $MgCl_2$ 500 ug/ml *p*-nitrophenylphosphate) was added into each well and the plate was put on a plate reader. The results were analyzed. (See Yu *et al*., 1996).

Establishing Human Tumor Xenografts Models in Mice

ICRSC-M SCID female outbred mice Taconic (Germantown, NY) were inoculated s.c. in the shoulder with 5×10^6 MDA-MB-231 cells or 1×10^7 TXM13 cells. It took eight weeks for MDA-MB231 tumors to reach an appropriate 1-cm size while twelve weeks for TXM13 tumor. All animal experiments were conducted in compliance with the Guidelines for the Care and Use of Research Animals established by the Institutional Animal Care and Use Committees at Washington University, The University of Missouri, and Harry S. Truman Veterans Hospital.

Imaging of Tumor Models with AF680 Conjugated Phage

The SCID mice with human tumors were chemically depilated over lesions 24 hrs prior to imaging procedure to minimize auto fluorescence on and around the tumor area. The mice were injected with 10^{11} virons of AF680 conjugated phage intravenously and the fluorescence imaging was acquired by the IVIS imaging system (Xenogen Corp., Alameda, CA) before and after the injection (1 hr, 2 hr, 4 hr, 6 hr and 24 hr) when the animals were under gas anesthesia. The fluorescence was measured and analyzed using corresponding software from Xenogen.

Peptide Synthesis

Amino acids and amide resin were purchased from Advanced ChemTech Inc. (Louisville, KY). DOTA- tri-t-butyl ester was purchased from Macrocyclic, Inc. (Richardson, TX). DOTA- tri-t-butyl ester was coupled to the N-terminus of

the peptide during the terminal round of synthesis using Fmoc/HBTU method on amide resin with a Synergy 432A desktop solid-phase peptide synthesizer (Applied Biosystems, Foster City, CA) in the combinatory biology core at the University of Missouri-Columbia.

Peptide Radiolabeling and Purification

The DOTA conjugated peptides were dissolved in distilled water (1 mg/ml). 30 μL $^{111}InCl_3$ in 0.05 mol/L HCl (Mallinckrodt, St. Louis, MO); 80 μL pH 5, 0.1 mol/L NH_4OAc; and 10 μg peptide were mixed and incubated at 80°C for 45 min. The radiolabeled complex was purified by reverse-phase high-performance liquid chromatography (RP-HPLC) (ProTeam LC, Phoenix, AZ) on a C-18 reverse-phase analytic column using a 20-min gradient of acetonitrile in 20 mmol/L HCl at a flow rate of 1 mL/min. This process was monitored with an ultraviolet flow detector and analytical radioactivity detector. The purified peptide samples were purged with N_2 gas for 15 min to remove the acetonitrile.

For the nonradioactive Indium-DOTA-peptide complexes, Indium (III) chloride tetrahydrate (Catalog Number. 22519-64-8, Aldrich Inc., St. Louis, MO) was added in ten fold molar excess Indium (III) chloride tetrahydrate to DOTA conjugated peptide in 0.1 M NH_4OAc, pH 5 solution. Reaction was heated at 80°C for 45 min. The complex was subjected to RP-HPLC and monitored by a UV absorption at 214 or 280 nm.

Cell Binding Assay with Synthetic Peptides

TXM13 and MDA-MB-231 were cultured as described above. Cells were detached by cell dissociation buffer, and placed in binding medium containing MEM, 25 mmol/L *N*-(2-hydroxyethyl) piperazine-*N*-(2-ethanesulfonic acid) (Sigma), 0.2% BSA, and 0.3 mmol/L 1, 10-phenanthroline(Sigma). One million cells were mixed with 10^6 cpm of radioactive peptide complexes or additional 1uM of non radioactive peptide complex for 90 min in binding medium in 1.5 ml tube and incubated at room temperature. The cells were recovered by centrifugation and washed with 1ml PBS for three times. Retained radioactivity was measured by gamma counter.

RESULTS

Bacteriophage Display Affinity Selection

In this study, three phage libraries developed from filamentous phage fd strain (f88-15mer, f88-15mer-cys6 and f3-15mer) were injected into mice. After 2h, the remaining phage in the blood were collected to form pre-cleared libraries. The pre-cleared phage libraries were also preselected against human melanocyte and breast epithelial 184A1 cell lines to reduce the population that can bind to these two normal cell lines. For the positive selection experiment, human melanoma TXM13 cells or breast cancer MDA-MB231 cells were magnetically labeled with tumor specific antibodies and loaded into column in a magnetic field. The phage libraries were applied in the column with tumor cells and unbound phage were washed away. Tumor cell bound phage were collected and amplified as input for next round selection. The output of each round was titered to monitor the stringency of selection. The yields and enrichment factors are shown in Table1.

An additional competition step was done in the second round of melanoma selection. Alpha-melanocyte stimulating hormone (α-MSH) is a well characterized peptide that binds to the melanocortin-1 receptor (MC1-R) which is upregulated in human melanoma cells (Siegrist *et al.*, 1989). It was pre-incubated with TXM13 cells and thus excluded the peptides bound to the MC1-R. Four rounds of selection were performed and 32 phage clones were randomly chosen for sequencing (Table 2). We obtained clones from all three libraries on both

TXM13 and MDA-MB-231 cells selection. These sequences were searched against nr protein sequence database on the NCBI website using Basic Local Alignment Search Tool (BLAST) and compared to our laboratory's phage–peptide sequence database (not published). We found that these sequences were unique sequences that were never published before. Three clones QADGPNSVVRPFTLT, PFARAPVEHHDVVGL and RVVDCHPGSSGALIC were in our lab database. These clones might be contaminated clones. Several clones contained RGD motifs in their sequences. We also compared to melanoma genomic signature genes such as β3 integrin, syndecan-4, WNT5a, MITF, tyrosinase, dopachrome tautomerase, DCT, melan-A and S100B (Tímár *et al*., 2006). No similarity was found. There were 18 sequences that appeared more than once, and these 18 phage clones were used as sources for next selection procedure.

Second Screen by Cell Based ELISA

The 18 clones from phage display selection were derivatized with biotin for ELISA. The cancer and normal cell lines were cultured to reach confluency on 96 well ELISA plates. Bound phage were quantified based on assay on alkaline phosphotase conjugated streptavidin. The results are shown in Figure 1. The

Table1. Yield and enrichment factors for phage display selection on melanoma and breast cancer cell lines.

Library/ Cell		Round 1	Round 2	Round 3	Round 4
f3-15mer/Mel	Yield=100 × (total number of output TUs)/(total number of input TUs)	1.00E-03	9.36E-04	8.58E-04	1.95E-03
f3-15mer/Brst		3.90E-04	8.23E-03	1.38E-02	4.60E-05
f88-15mer/Mel		3.31E-03	8.14E-04	2.26E-03	5.01E-03
f88-15mer/Brst		4.38E-04	3.49E-03	1.59E-02	5.66E-03
f88-Cys6/Mel		2.47E-03	5.57E-04	6.48E-03	4.77E-03
f88-Cys6/Brst		3.75E-03	1.07E-02	1.93E-02	1.57E-05
f3-15mer/Mel			4.17E-04	1.64E-04	5.87E-04
f3-15mer/Brst			5.77E-03	8.34E-03	6.31E-06
f88-15mer/Mel			2.76E-04	2.28E-04	2.09E-03
f88-15mer/Brst			1.07E-03	7.64E-03	1.28E-04
f88-Cys6/Mel			1.32E-04	5.78E-04	2.38E-03
f88-Cys6/Brst			8.24E-03	3.17E-02	1.07E-05
f3-15mer/Mel	Enrichment= (percent yield of library phage)/(percent yield of control phage)		2.25E+00	5.23E+00	3.32E+00
f3-15mer/Brst			1.43E+00	1.65E+00	7.30E+00
f88-15mer/Mel			2.95E+00	9.92E+00	2.40E+00
f88-15mer/Brst			3.25E+00	2.08E+00	4.40E+01
f88-Cys6/Mel			4.21E+00	1.12E+01	2.00E+00
f88-Cys6/Brst			1.30E+00	6.09E-01	1.47E+00

Mel is for melanoma and Brst is for breast cancer.

Table 2. Results of phage display selection against tumor cell lines: Deduced peptide sequences and frequency of phage clones.

Peptide	f3-15mer		f88-15mer		F88-Cys6	
	Mel	Brst	Mel	Brst	Mel	Brst
	29	13	27	9	23	6
	Number of clones encoding indicated peptide					
QADGPNSVVRPFTLT	1					
ACVGMSIHTSACASG	1					
GGGLTASGCVRYGMC	1					
SPGYGHGGSLWAASV	1					
PVQRSIFTGGNPYHA	1					
TDPYSSMPVVY	1					
RWSVQWGSRT	1					
AHCKLISSAKASPIG	1					
RVVDCHPGSSGALIC	1					
HGSLGLGWPGHTSVR	1					
PNQRSDVSSFWPIDP	1					
GSYGGLRADPREAGP	1					
IESWVVAEG	1					
VQARPVESPRLDRLR	1					
STSCGVAYSCAYRHV	1					

RVGDRMRTGIDSSHR	1					
ITVSRASDTSSDFFS	1					
AFNQGTFTGRFSSPA	1					
EGGPPLLAGRLPGSS	1					
HVGPCSFQSARSCGV	1					
GDSLHSADGATSRFY	3					
GIHSNSFGLGDVAYS	6	2				
DRCSSDHTWSRLCMY		2				
W		1				
PFARAPVEHHDVVGL		1				
SSPKQRANFGMASPD		1				
GRG		1				
KLRDRINFLHHSDYH		1				
VWWRALLVFATLYSV		1				
APGPLGWGYGGRVAA		1				
MHFGPGFGH		1				
GDSGDRSLSVQSLGV		1				
GTAPSLLDDPWQPHT			6			
RGDMGWMAAGHSTPS			5			
SQKTNLHLEPSPQGL			2			
RGDMPSALALPSAHT			2			
SLNGRNTDFPSPPFR			2			
QVPLSLWTGQYDFDS			2			

GLNGRYDPLQTTSPP			2			
RSMPPLPLLEPFP			1			
...CRSDVCTLRWPA			1			
....DSFMCLASTEL			1			
...RPTPTTPSRMLA			1			
...CLFRFRRSVCSC			1			
....RSMPPLPLLEP			1			
DYPVLVMTGMEGALK				4		
QKPEMSAGGAHWAWI				3		
DKYKGQEGSWHWSVS				1		
ARDKCIYGQPHCTSEM					7	
SKQTCRGDMCVSLRG					4	
AEEPKWIMLRSGVWRLG					2	
CRGDCFMANEYVLFGR					2	
ELIDCMDLWTQCLDAA					2	
IGHNCSTNMNPCHAEW					1	
LNGRCDPTLIKCSQET					1	
NVTSCPRGDAPCRMQQ					1	
DHKTCRKQYKNCQLGI					1	
EPVYCNCRTDACWECT					1	
RTQHCRGDNYNCMQTA					1	
RMPPCNDDFPWCEHLY						2
HPRSCLTWESNCPQQS						1

AVSNCVEEGPWCEMTV						1
DTPKCDLMGPVCRIYL						1
DMITCGEPNNWCGNTT						1
....*YSPEGNRLPG			1			
.....SF*PQPLRSI			1			
GMAVQCSTTENRC*MPP					1	
TRWWCVDQMKSCQ*KA					1	
AKR*LSIFMSV*LCFp				1		
EYGMCTD*KPGCWVLSA					1	
K*TVCHYNFLICEDPW						1
CNTGC*FIGVYCSQTMPp						1

*Star represents stop cordon. The frequency of phage clones is the number of clones over total clones sequenced, which is 32. Mel is for melanoma cell lines and Brst is for breast cancer cell lines.

Figure 1. Cell based ELISA of phage clones. 18 phage clones (M1-M18) selected from phage display on melanoma and breast carcinoma, together with negative control phage fd were examed for binding to melanoma cells (A), melanocyte (B), breast carcinoma cells (C) and breast epithelial cells (D). Biotinylated phage were added into 96 well ELISA plates containing cells grown to confluency in RPMI1640. After 1h incubation at 37 ^{o}C, the cells were washed three times using washing buffer (1mM $CaCl_2$, 0.5mM $CaCl_2$, 1%BSA in TBS). 200ng/ml AP-SA(alkaline phophotase conjugated streptavidin) in washing buffer was added into each well and after 30 min, 0.5 mg/ml NPP (*p*-nitrophenylphosphate) in 1M diethanolamine buffer pH 9.8, 1 mM $MgCl_2$ solution was added to the plates and subject to a plate reader immediately to determine absorbance values at 410nm.

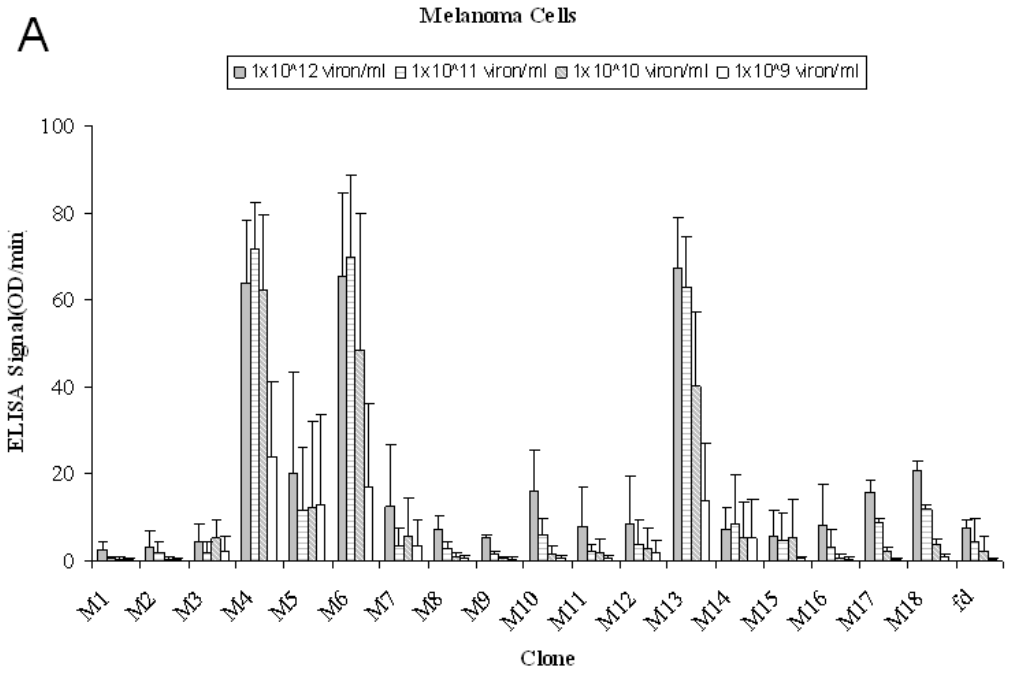
A
Melanoma Cells
1x10^12 viron/ml
1x10^11 viron/ml
1x10^10 viron/ml
1x10^9 viron/ml
ELISA Signal(OD/min)
100
80
60
40
20
0
M1
M2
M3
M4
M5
M6
M7
M8
M9
M10
M11
M12
M13
M14
M15
M16
M17
M18
fd
Clone

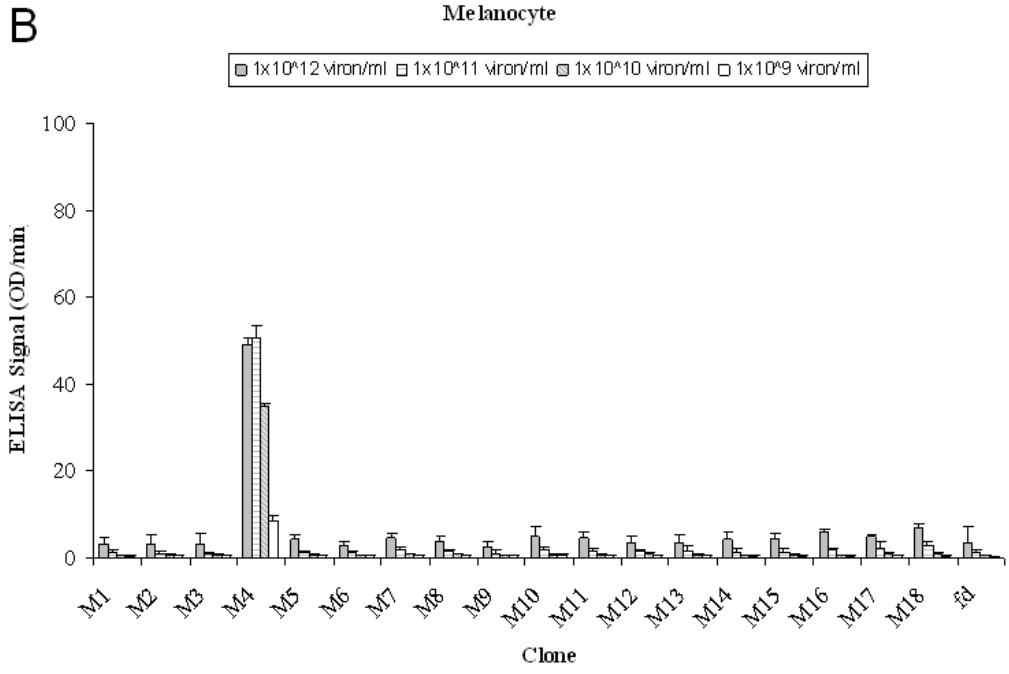
B
Melanocyte
1x10^12 viron/ml
1x10^11 viron/ml
1x10^10 viron/ml
1x10^9 viron/ml
ELISA Signal (OD/min)
100
80
60
40
20
0
M1
M2
M3
M4
M5
M6
M7
M8
M9
M10
M11
M12
M13
M14
M15
M16
M17
M18
fd
Clone

C

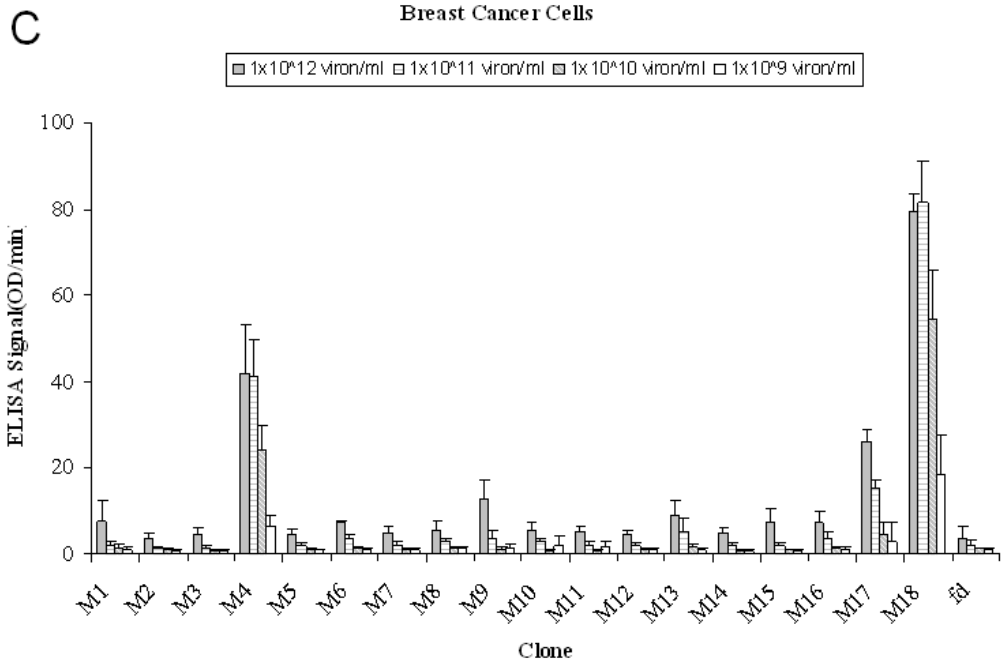
Breast Cancer Cells
1x10^12 viron/ml
1x10^11 viron/ml
1x10^10 viron/ml
1x10^9 viron/ml
ELISA Signal(OD/min)
100
80
60
40
20
0
M1
M2
M3
M4
M5
M6
M7
M8
M9
M10
M11
M12
M13
M14
M15
M16
M17
M18
fd
Clone

D

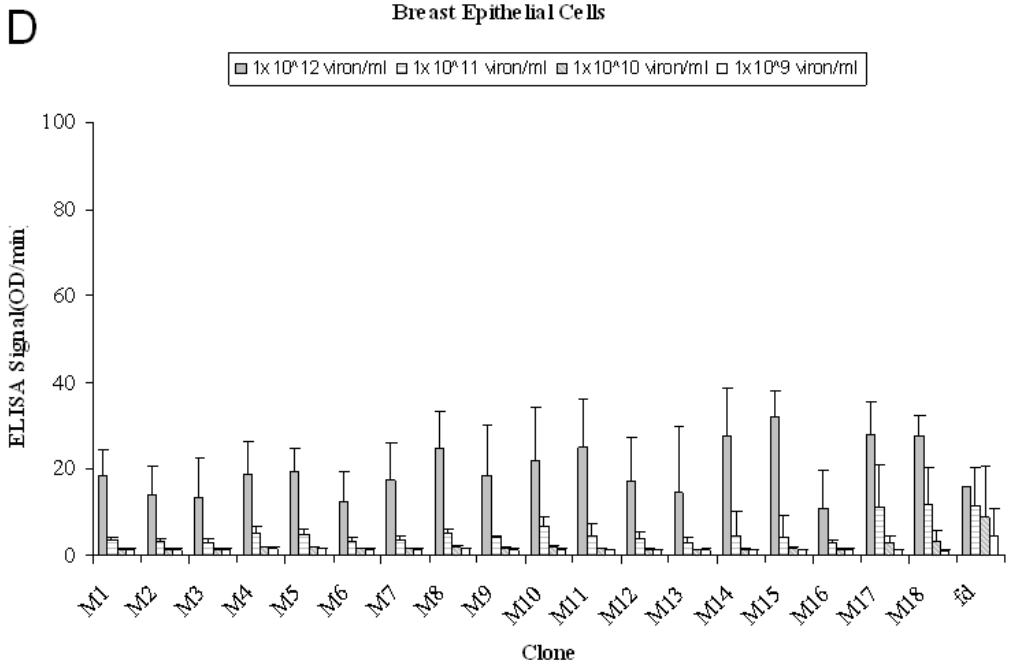
Breast Epithelial Cells
1x10^12 viron/ml
1x10^11 viron/ml
1x10^10 viron/ml
1x10^9 viron/ml
ELISA Signal(OD/min)
100
80
60
40
20
0
M1
M2
M3
M4
M5
M6
M7
M8
M9
M10
M11
M12
M13
M14
M15
M16
M17
M18
fd
Clone

clones M6, M13 and M18 had ~30 fold more binding affinity compared to the fd control phage. M4 was probably a false positive clone since it bound at an intermediate signal level in the normal cell line.

Live Animal Fluorescent Analysis

The 18 phage clones were labeled with AlexFlour 680 and injected into mice. Fluorescence signal acquisition was performed prior to phage injection, and 1, 2, 4, and 6 h after injection. Figure 2 is an example of the fluorescence imaging. Figure 2A shows a fluorescent image from M7 clone injected into TXM13 bearing mice. Figure 2B is a quantitation of Figure 2A, while Figure 2C is quantitation of negative control phage fd. Fluorescence accumulation was used as standard to divide the phage clones into two groups: one was the group of phage clones with 2 fold increase in fluorescence intensity accumulated in tumor over intrinsic fluorescence intensity of tumor prior injection, and another group of phage clones that did not have a significant change of fluorescence intensity relative to fd control phage. The six-amino-acid peptide, KCCYSL, which targets HER2, was used as a positive control for the in vivo fluorescence assay (Kumar *et al*., 2007). The results for the fluorescence assay to 32 phage clones are listed in Table 1. Three phage clones (M4, M7, and M9) showed at least a fold greater fluorescence signal post injection compared over pre-injection on melanoma mouse models, while 6 clones (M1, M2, M3, M6, M13 and M18) were identified from breast carcinoma models.

Figure 2. Live animal fluorescent imaging of phage clone M7 and fd. Phage clone M7 labeled with Alex Fluor 680 was injected into mice bearing TXM13 tumors. At various times 1h, 2h, 4h, 6h, 24h after injection, the animals were assayed using optical live animal imaging device (Xenogen). Figure 2A shows the animal imaging at different time points. 0h means the imaging prior to phage injection. The circles indicated tumors in mice. 2B Quantitation of fluorescence intensity of fd (wide type phage) in TXM13 tumor over time 2C Quantitation of tumor fluorescence intensity for phage clone M7 (Figure 2A) over time

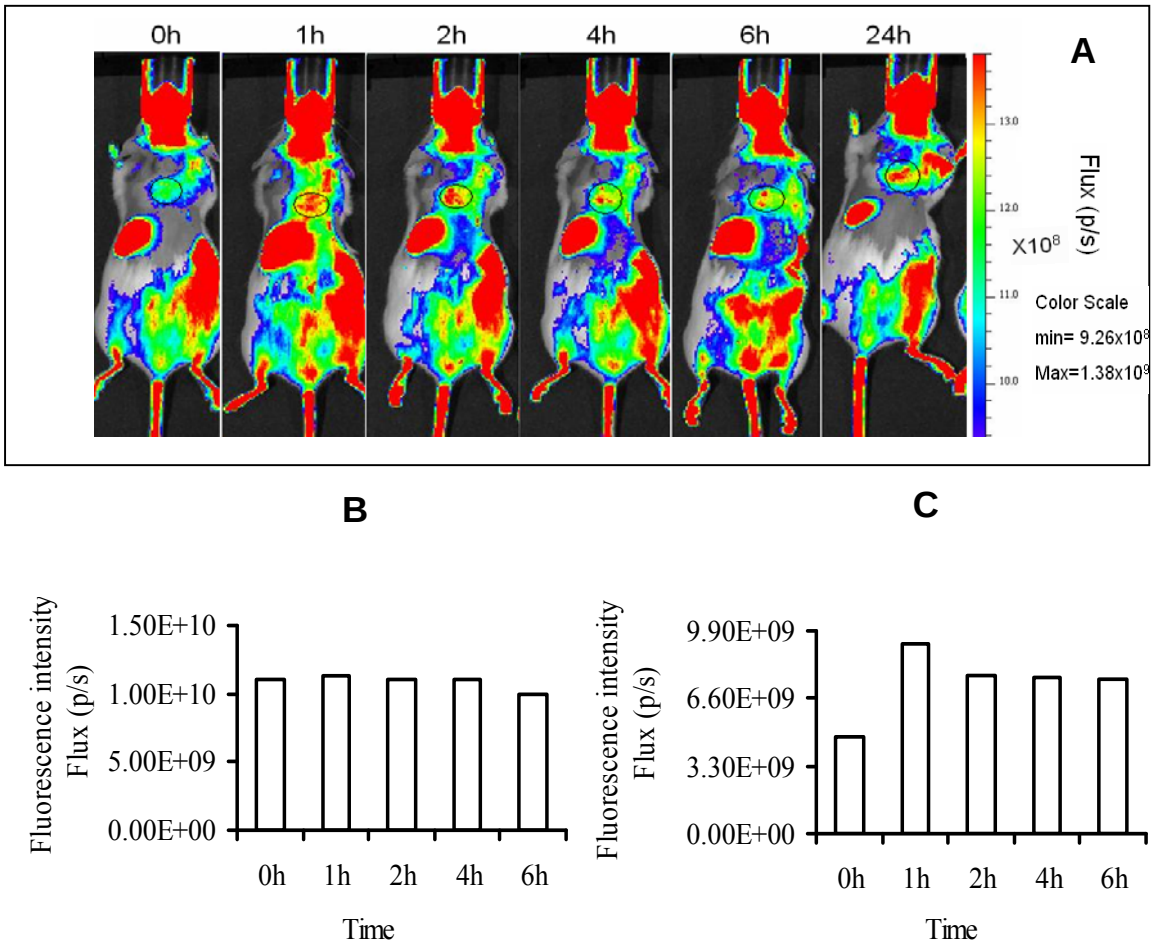
0h
1h
2h
4h
6h
24h
A
Flux (p/s)
X10^8
Color Scale
min= 9.26x10^8
Max=1.38x10^9
B
C
Fluorescence intensity
Flux (p/s)
1.50E+10
1.00E+10
5.00E+09
0.00E+00
0h
1h
2h
4h
6h
Time
Fluorescence intensity
Flux (p/s)
9.90E+09
6.60E+09
3.30E+09
0.00E+00
0h
1h
2h
4h
6h
Time

Table 3. Summary of phage candidate clones.

Clone Name	Library Used	Cell Lines Used	Freq u-ency	Peptide Sequence	*Mel Mouse Model	*Brst Mouse Model
M1	f3-15mer	*Mel, *Brst	6,2/32	GIHSNSFGLGDVAYS	*N	*Y
M2	f3-15mer	Mel	3/32	GDSLHSADGATSRFY	N	Y
M3	f3-15mer	Brst	2/32	DRCSSDHTWSRLCMY	N	Y
M4	f88-15mer	Mel	6/32	GTAPSLLDDPWQPHT	Y	N
M5	f88-15mer	Mel	5/32	RGDMGWMAAGHSTPS	N	N
M6	f88-15mer	Mel	2/32	SQTKNLHLEPSPQGL	N	Y
M7	f88-15mer	Mel	2/32	RGDMPSALALPSAHT	Y	N
M8	f88-15mer	Mel	2/32	SLNGRNTDFPSPPFR	N	N
M9	f88-15mer	Mel	2/32	QVPLSLWTGQYDFDS	Y	N
M10	f88-15mer	Mel	2/32	GLNGRYDPLQTTSPP	N	N
M11	f88-15mer	Brst	4/32	DYPVLVMTGMEGALK	N	N
M12	f88-15mer	Brst	3/32	QKPEMSAGGAHWAWI	N	N
M13	f88-15mer-	Mel	7/32	ARDKCIYGQPHCTSEM	N	Y
M14	f88-15mer-	Mel	4/32	SKQTCRGDMCVSLRG	N	N
M15	f88-15mer-	Mel	2/32	AEEPKWIMLRSGVWRL	N	N
M16	f88-15mer-	Mel	2/32	CRGDCFMANEYVLFGR	N	N
M17	f88-15mer-	Mel	2/32	ELIDCMDLWTQCLDAA	N	N
M18	f88-15mer-	Brst	2/32	RMPPCNDDFPWCEHLY	N	Y

* Mel is for melanoma cell lines and Brst is for breast cancer cell lines. Y means this clone has time dependent accumulation during fluorescent imaging study while N means the opposite.

Peptide Complexes and Purification

Five peptides were chosen to be further investigated based on the in *vitro* cell binding and in *vivo* fluorescence image assays described above (Table 4). The peptides were synthesized with a DOTA chelator on their N-termini and GSG amino acid linker between the DOTA and peptide. ^{111}In can coordinate with the backbone nitrogens and carboxyl groups of the DOTA chelator to form a stable structure when heated (Miao, 2003). The radiolabeled peptide was purified from excess non-radiolabeled peptide by RP HPLC.

Cell Binding Assay of peptides

Display phage of the f88 class contain about 100 copies of phage coat protein pVIII fused with peptides (Smith *et al*., 1997). This increases the local concentration of the displayed peptide compared to free peptides in solution. When a displayed peptide interacts with the cell surface, nearby coat proteins can influence the confirmation of the peptides or cell surface through and avidity effect. Thus the binding activities of phage clones may not guarantee the binding activities of synthetic peptides. In order to confirm the binding activities of the synthetic peptides, a competitive cell binding assay was performed. The In-DOTA-peptide non radioactive complexes were used in a competitive binding assay with ^{111}In-DOTA-peptide radioactive complexes to distinguish the specific binding activities. The competitive assays were performed on TXM13, MD-MBA -231 cells which were the cell lines used during the selection. Competitive binding assays were also performed on the B16 cells, a murine melanoma cell line

and MD-MB-435 cells, another invasive breast cancer cell lines. The human melanocyte and the breast epithelial cell line 184A1 were used as negative controls to estimate the background binding. The results of the competitive assays were shown in Figure 4. If the peptides can bind to tumor cells, the addition of the non radiolabeled peptide complex competes with the radiolabelled complex binding to the tumor cells and results in reduction in the amount of bound radiolabelled peptides on cells. Generally, M2 and M6 had a ~30% reduction on cancer cell lines in the blocking assay while M7, M13 and M18 had about 60% or more reduction on cancer cell lines in the blocking assay. M13 had a 75% reduction on both the TXM13 and B16 cell lines but had almost no reduction on the melanocyte cells. M7 and M18 had about 60% reduction on the MDA-MB-231 and MDA-MB-435 cells while no significant reduction on the 184A1 cells. The competitive binding assay results demonstrate that M7. M13, M18 have specific binding to the tumor cells and thus M13 is a potentially good imaging probe for melanoma while M7 and M18 are for breast cancer.

Table 4. Sequences of selected synthetic peptides

Peptide No.	Peptide Sequence	Clones No.
201-23	DOTA-GSG-GDSLHSADGATSRFY	M2
201-26	DOTA-GSG-SQTKNLHLEPSPQGL	M6
201-28	DOTA-GSG-RGDMPSALALPSAHT	M7
201-30	DOTA-GSG-ARDKCIYGQPHCTSEM	M13
201-32	DOTA-GSG-RMPPCNDDFPWCEHLY	M18

Figure 3. RP HPLC purification of radiolabeled peptide complexes. Figure 3 (A)-(E) show the RP-HPLC purification chromatography traces of the peptide M2, M6, M7, M13, M18 peptides respectively. In each figure, the upper portion of the graph was from the radioactivity detector and the lower part was from the UV detector. All the peptides were monitored at 214nm except M18 which was monitored at 280nm. The peptides were purified via RP-HPLC using a 20-min gradient of acetonitrile (with 0.01% TFA) in 20 mmol/L HCl at a flow rate of 1 mL/min. The gradient profiles were 28-35% for M2 and M7, 28-32% for M6, 26-32 for M13 and 32-42% for M18. The radiolabeled peptide complexes were collected when the UV signals decreased to about half of maximum.

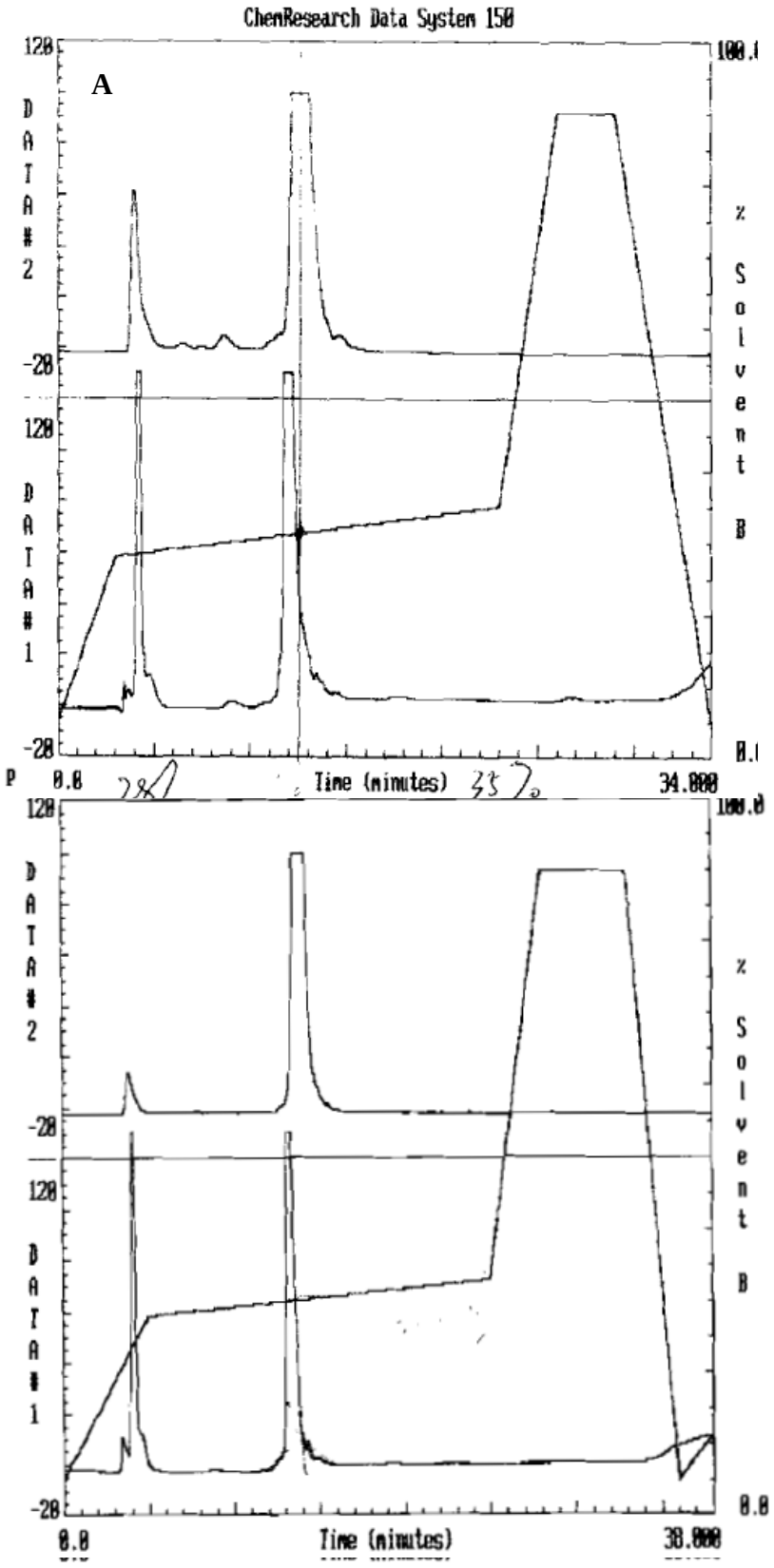
ChemResearch Data System 150
A
DATA#2
DATA#1
% Solvent B
Time (minutes)
0.0
34.000
30.000

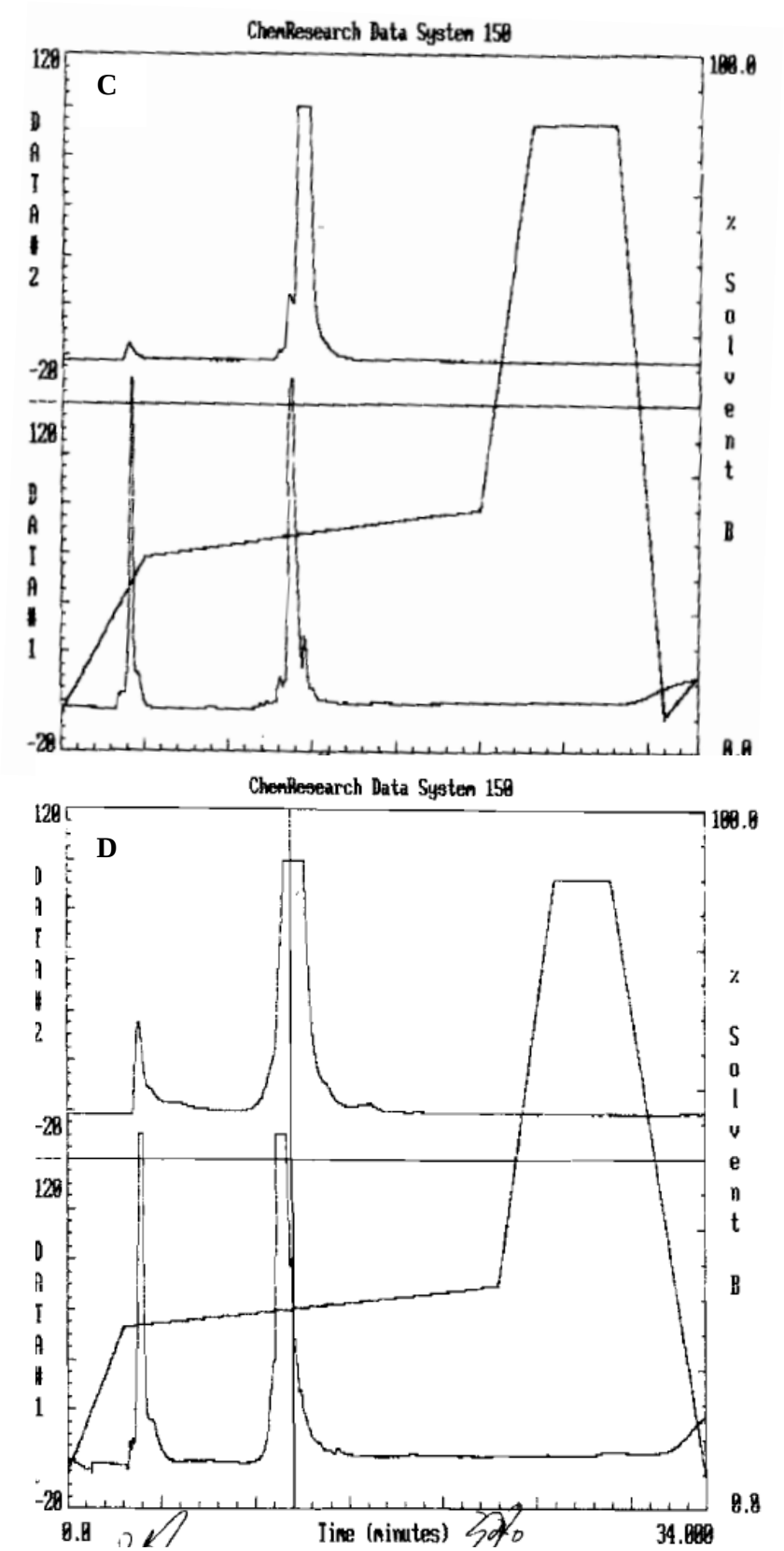
ChemResearch Data System 150
C
120
-20
DATA #2
120
-20
DATA #1
100.0
% Solvent B
0.0
ChemResearch Data System 150
D
120
-20
DATA #2
120
-20
DATA #1
100.0
% Solvent B
0.0
0.0
Time (minutes)
34.000

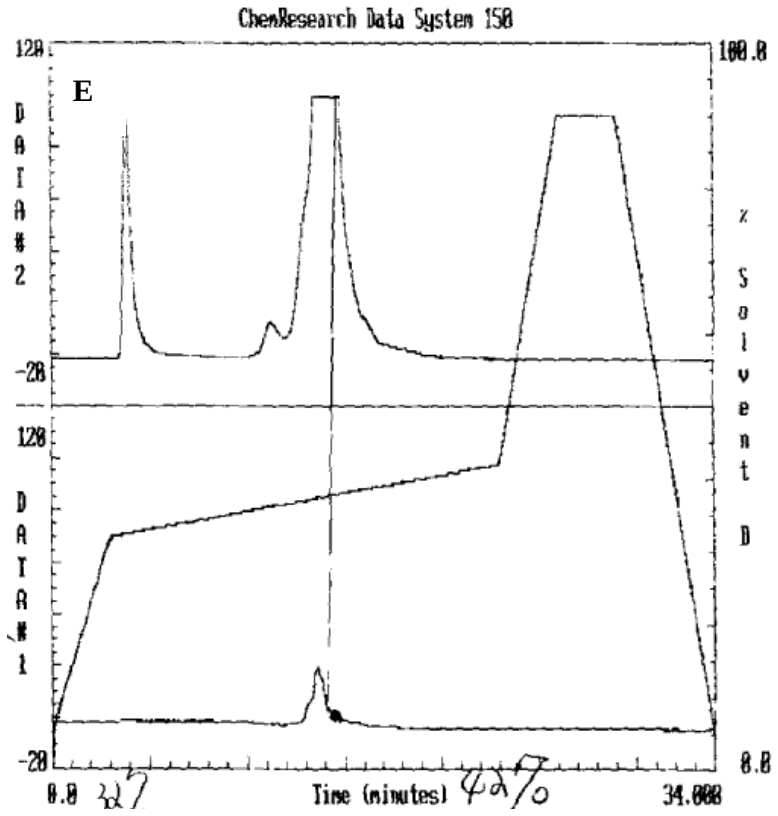
ChemResearch Data System 150
E
DATA #2
DATA #1
% Solvent D
Time (minutes)
34.000
0.0
100.0
0.0
128
-28

Figure 4. Cell binding assays of radiolableled peptides. The ^{111}In-DOTA-peptide complexes were purified by RP-HPLC. One million cpm of each complex was mixed with 1,000,000 cells and incubated for 90 min. As a blocking assay, In-DOTA-peptide cold complex 1 μmol was added to the tubes in addition to the ^{111}In-DOTA-peptide. After the incubation, the mixtures were washed by PBS with 0.02% BSA three times and the absorbed radioactivities by cells were measured. Five peptides M2, M6, M7, M13 and M18 were used on two human breast cancer cell lines MDA-MB231 and MDA-MB-435, mouse melanoma cell line B16, human melanoma cell line TXM13, human non cancer cell line melanocyte and breast epithelial cells 184A1.

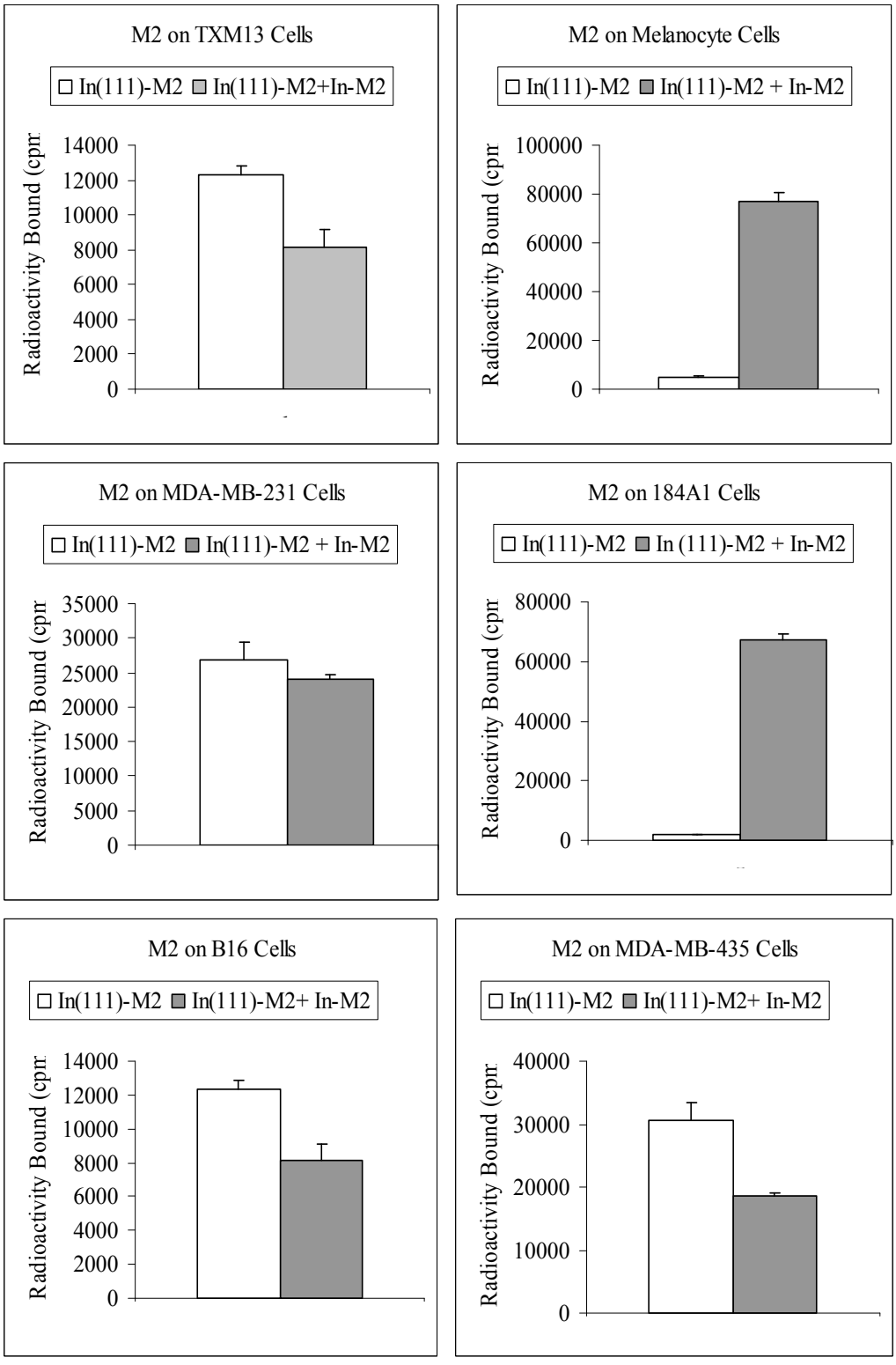
M2 on TXM13 Cells
In(111)-M2
In(111)-M2+In-M2
Radioactivity Bound (cpm
14000
12000
10000
8000
6000
4000
2000
0
M2 on Melanocyte Cells
In(111)-M2
In(111)-M2 + In-M2
Radioactivity Bound (cpm
100000
80000
60000
40000
20000
0
M2 on MDA-MB-231 Cells
In(111)-M2
In(111)-M2 + In-M2
Radioactivity Bound (cpm
35000
30000
25000
20000
15000
10000
5000
0
M2 on 184A1 Cells
In(111)-M2
In (111)-M2 + In-M2
Radioactivity Bound (cpm
80000
60000
40000
20000
0
M2 on B16 Cells
In(111)-M2
In(111)-M2+ In-M2
Radioactivity Bound (cpm
14000
12000
10000
8000
6000
4000
2000
0
M2 on MDA-MB-435 Cells
In(111)-M2
In(111)-M2+ In-M2
Radioactivity Bound (cpm
40000
30000
20000
10000
0

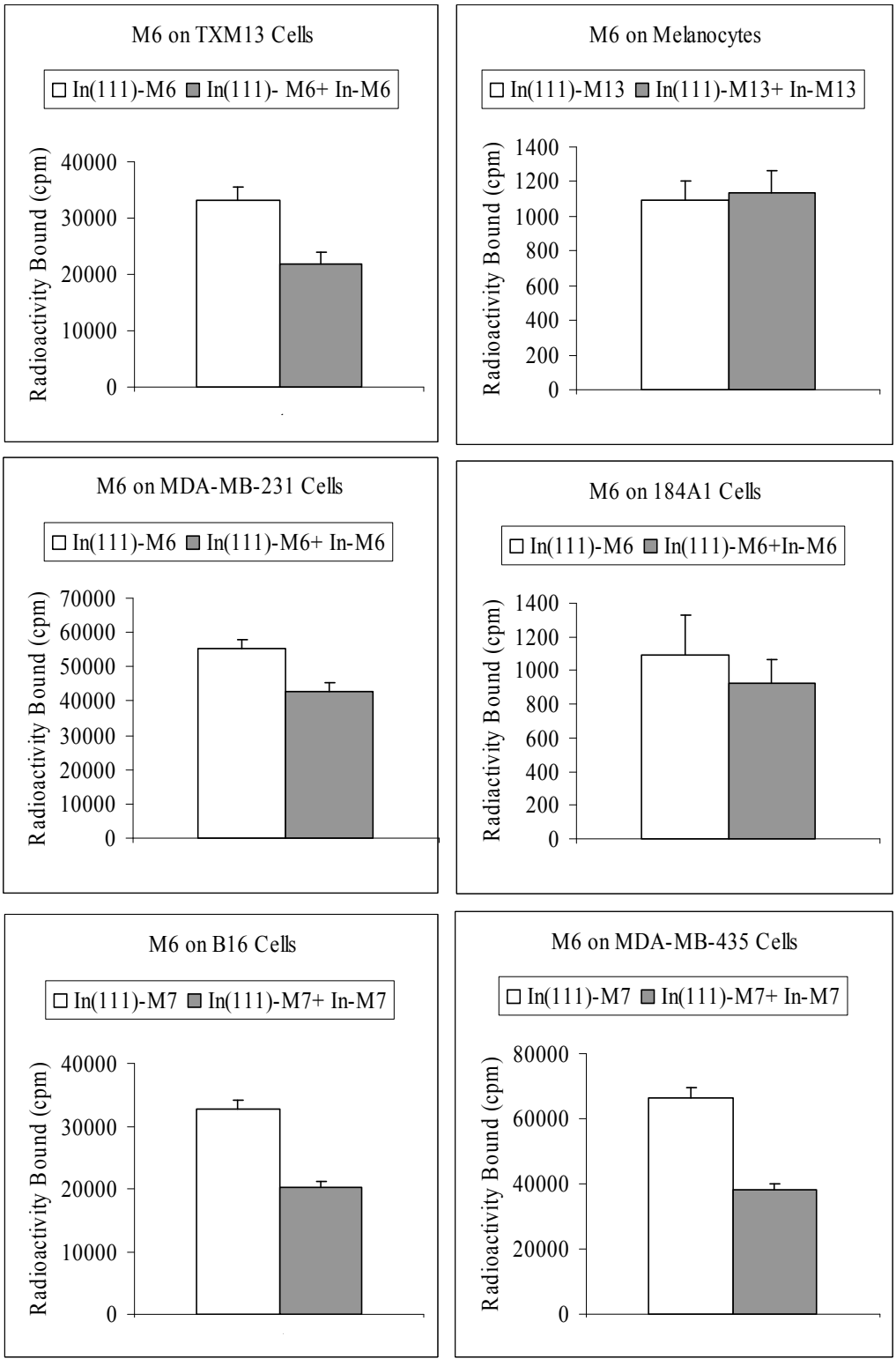
M6 on TXM13 Cells
In(111)-M6
In(111)- M6+ In-M6
Radioactivity Bound (cpm)
40000
30000
20000
10000
0
M6 on Melanocytes
In(111)-M13
In(111)-M13+ In-M13
Radioactivity Bound (cpm)
1400
1200
1000
800
600
400
200
0
M6 on MDA-MB-231 Cells
In(111)-M6
In(111)-M6+ In-M6
Radioactivity Bound (cpm)
70000
60000
50000
40000
30000
20000
10000
0
M6 on 184A1 Cells
In(111)-M6
In(111)-M6+In-M6
Radiactivity Bound (cpm)
1400
1200
1000
800
600
400
200
0
M6 on B16 Cells
In(111)-M7
In(111)-M7+ In-M7
Radioactivity Bound (cpm)
40000
30000
20000
10000
0
M6 on MDA-MB-435 Cells
In(111)-M7
In(111)-M7+ In-M7
Radioactivity Bound (cpm)
80000
60000
40000
20000
0

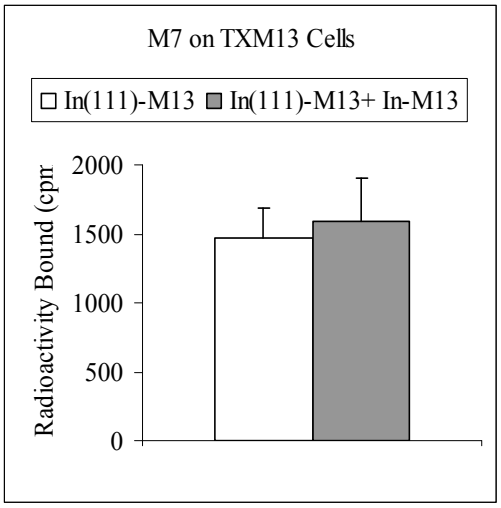
M7 on TXM13 Cells
In(111)-M13
In(111)-M13+ In-M13
Radioactivity Bound (cpm
2000
1500
1000
500
0

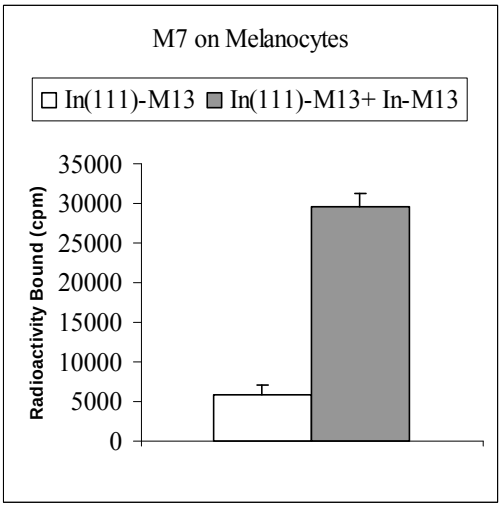
M7 on Melanocytes
In(111)-M13
In(111)-M13+ In-M13
Radioactivity Bound (cpm)
35000
30000
25000
20000
15000
10000
5000
0

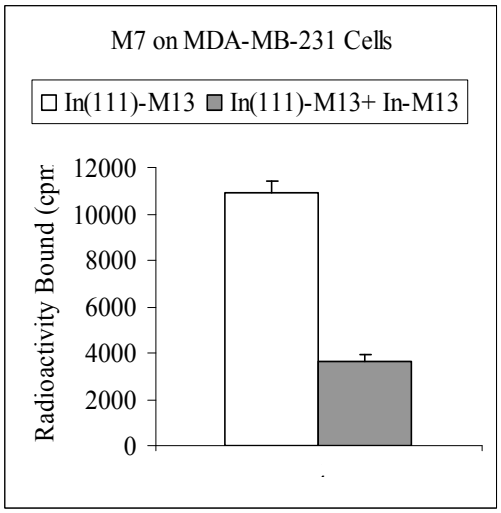
M7 on MDA-MB-231 Cells
In(111)-M13
In(111)-M13+ In-M13
Radioactivity Bound (cpm
12000
10000
8000
6000
4000
2000
0

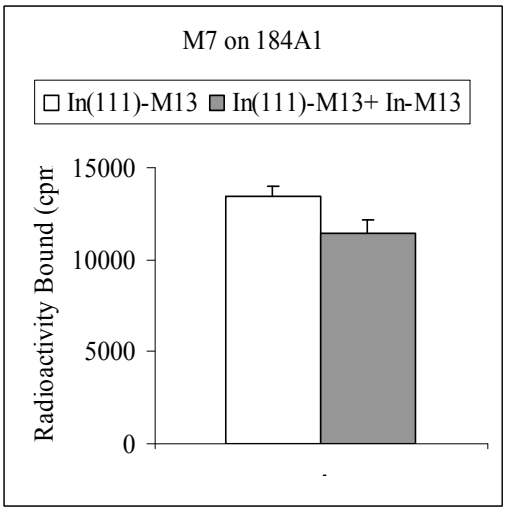
M7 on 184A1
In(111)-M13
In(111)-M13+ In-M13
Radioactivity Bound (cpm
15000
10000
5000
0

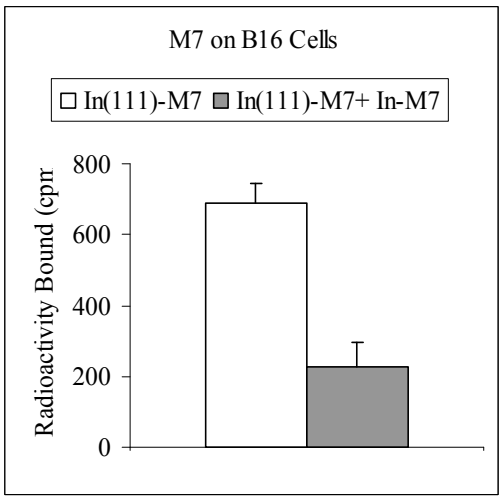
M7 on B16 Cells
In(111)-M7
In(111)-M7+ In-M7
Radioactivity Bound (cpm
800
600
400
200
0

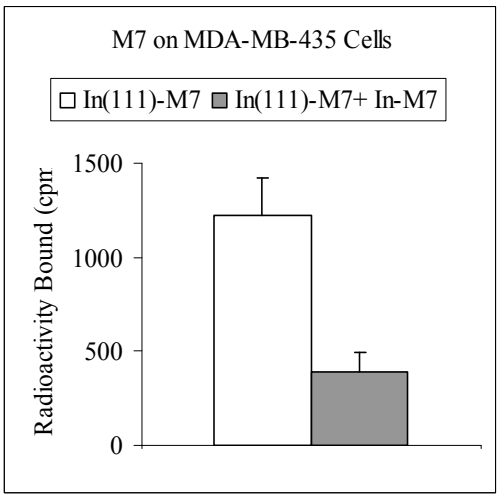
M7 on MDA-MB-435 Cells
In(111)-M7
In(111)-M7+ In-M7
Radioactivity Bound (cpm
1500
1000
500
0

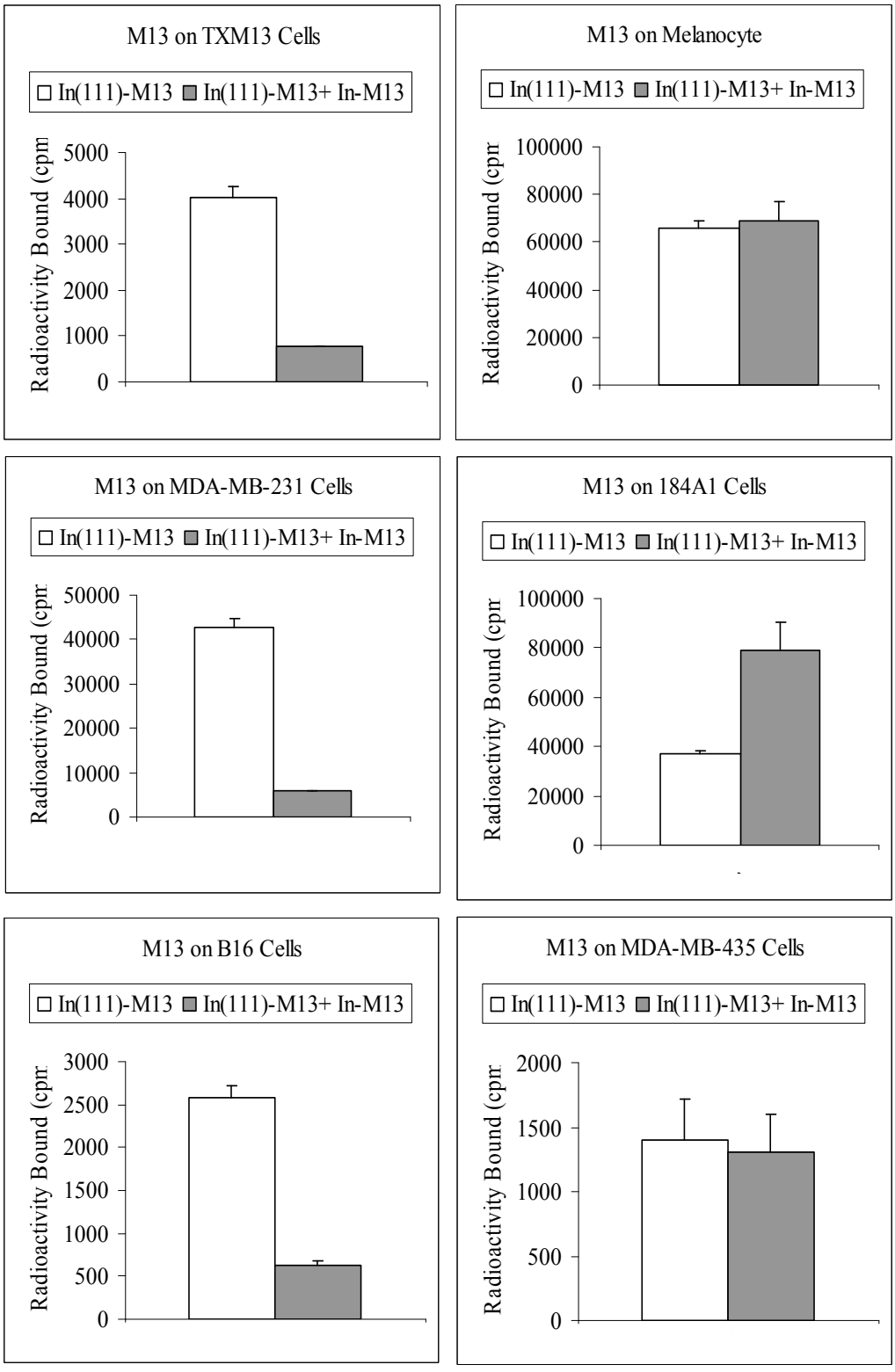
M13 on TXM13 Cells
In(111)-M13
In(111)-M13+ In-M13
Radioactivity Bound (cpm
5000
4000
3000
2000
1000
0
M13 on Melanocyte
In(111)-M13
In(111)-M13+ In-M13
Radioactivity Bound (cpm
100000
80000
60000
40000
20000
0
M13 on MDA-MB-231 Cells
In(111)-M13
In(111)-M13+ In-M13
Radioactivity Bound (cpm
50000
40000
30000
20000
10000
0
M13 on 184A1 Cells
In(111)-M13
In(111)-M13+ In-M13
Radioactivity Bound (cpm
100000
80000
60000
40000
20000
0
M13 on B16 Cells
In(111)-M13
In(111)-M13+ In-M13
Radioactivity Bound (cpm
3000
2500
2000
1500
1000
500
0
M13 on MDA-MB-435 Cells
In(111)-M13
In(111)-M13+ In-M13
Radioactivity Bound (cpm
2000
1500
1000
500
0

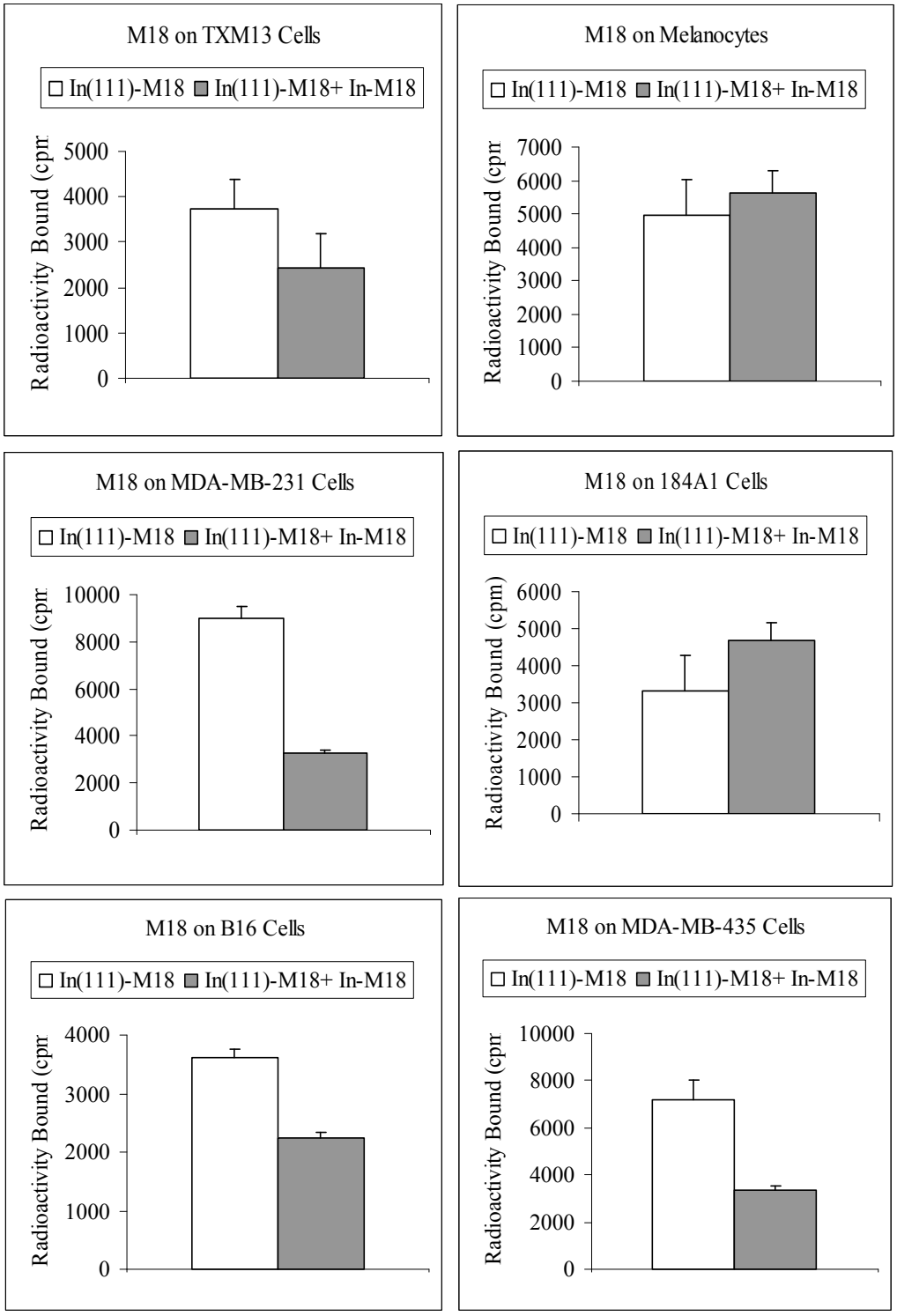
M18 on TXM13 Cells
□ In(111)-M18 ■ In(111)-M18+ In-M18
Radioactivity Bound (cpm
5000
4000
3000
2000
1000
0
M18 on Melanocytes
□ In(111)-M18 ■ In(111)-M18+ In-M18
Radioactivity Bound (cpm
7000
6000
5000
4000
3000
2000
1000
0
M18 on MDA-MB-231 Cells
□ In(111)-M18 ■ In(111)-M18+ In-M18
Radioactivity Bound (cpm
10000
8000
6000
4000
2000
0
M18 on 184A1 Cells
□ In(111)-M18 ■ In(111)-M18+ In-M18
Radioactivity Bound (cpm)
6000
5000
4000
3000
2000
1000
0
M18 on B16 Cells
□ In(111)-M18 ■ In(111)-M18+ In-M18
Radioactivity Bound (cpm
4000
3000
2000
1000
0
M18 on MDA-MB-435 Cells
□ In(111)-M18 ■ In(111)-M18+ In-M18
Radioactivity Bound (cpm
10000
8000
6000
4000
2000
0

DISCUSSION

The goal of the study was to select peptides as potential molecular probes in cancer imaging of melanoma and breast carcinoma using phage display technology. In the medical imaging process, the signal-noise ratio is important for the clarity of the imaging. One way to improve the signal to noise ratio is to use peptides with high affinity for the tumor, while maintaining the low binding on the other organs and tissues. During our selection, in order to reduce non specific binding to the vasculature, the phage libraries were injected in mice intravenously and collected the fraction in blood as mouse pre-cleared libraries. We further incubated the mouse pre-cleared libraries with human noncancer cell lines to enhance the tumor specificity. First of all, most imaging agents are injected intravenously in human body in clinical use, and thus they are exposed to the circulation system for a long time before they actually reach the tumor site. They are excreted either by hepatobiliary route or by the kidney. Ideally, nontumor binding activity should be the minimum if the phage libraries could be pre-incubated with all the possible human normal organs and tissues, although this is not practical. We did use the mouse vessel pre-cleared libraries to initiate our selection, which contained very few if any vessel binding clones. From the sequencing results shown in Table 2, the RGD motifs among the sequences that are not predominant, which were originally selected as tumor vasculature binding motif (Pasqualini *et al*., 1996). The presence of RGD sequences possibly partially could be due to the insufficiency of the depletion procedure. Since the RGD motif

binds to αvβ3 integrin, an adhesion molecule abundant on tumor cells as well, we could not exclude the possibilities that these peptides could bind to tumor (Van der Flier *et al*., 2001).

Secondly, pre-incubation of the mouse vessel depleted libraries was performed to reduce clones that bound normal cell surface receptors. In the cell binding assays with the 18 repeated clones from the selection (Figure 1), one clone M4 showed higher signal strength on breast cancer cells and melanoma cells as well as the melanocytes, which indicated it had no tumor specificity. The other clones had nearly identical ELISA signals as the negative control phage fd on the human normal cells. So the human non cancer cell depletion procedure appeared to improve the tumor specificity of selection.

The pitfall of the intensive depletion procedures prior to positive selection is the loss of potentially interesting phage clones that bind to the tumor cells specifically. This can be analyzed by monitoring the representation of the output. The library's diversity can be reflected by the number of the primary clones in the original library. The "representation" is the number of infected cells amplified per primary clone. The higher the representation, the more fully the diversity of the original library is preserved during amplification. The representations of the three libraries from the output of the mouse depletion procedure were from 22 to 360. The representations of those from the noncancer human cell depletion were from 43 to 305. Therefore, even the yield of the two depletion procedures were low but they are still high enough to give reasonable representations, which indicated

that most of the diversity of the original library were preserved in the mouse depletion process.

Our group has been working with the alpha-melanocyte stimulating hormone (α-MSH) peptide derivatives during the last 15 years to develop then for clinical use. Wild type MSH peptide was a natural human peptide used to regulate skin pigmentation. Its receptor, melanocortin-1 receptor (MCR1), was upregulated in human melanoma cells making it a good target for imaging and therapy (Sawyer *et al*., 1990; Siegrist *et al*., 1989). One of the analogs of α-MSH, Re(Arg^{11})CCMSH, had a high affinity for the MCR1 at nM level. (Miao *et al.,* 2003) However, there are only a limited number of MCR1 receptors present on human melanoma cells (900 to 5700 per cell), which requires that the radiolabel MSH analogs be prepared at high specific activities using RP-HPLC. The reaction chemistry and the RP-HPLC purification are not easily performed in the clinic, making the preparation of the radiolabeled melanoma targeting peptides in medical diagnosis difficult. So one of our important goals was to identify new melanoma specific peptides with high affinity that could be effected radiolabeled. During the second round of phage selection, we used the excessive Re(Arg^{11})CCMSH peptide to block the MCR1 receptors. The MCR1 blocking step was apparently successful since no sequences were identified that contains the CCMSH motif.

After we performed phage display *in vitro* screens by MACS, we found 18 clones showed a frequency higher that 2/32 when sequenced. There was no

common motif among the peptide sequences from the phage display selection. This indicates the low stringency or insufficient amount of clones sequenced. Only 32 clones were chosen to be sequenced and it is possible that the bias eliminates the clones of high frequency clones. Additional rounds of selection can be performed to improve the stringency of the selection. However, the practice of the selection technique will limit the stringency. When the stringency is too high, the background yield would be too high and thus the favorable binding is buried (Smith et al., 1997). Additional rounds of selection may be helpful to reveal novel clones.

To continue, the 18 selected phage clones of higher frequency in sequencing results were used *in vitro* cell binding assays and in *vivo* animal fluorescence studies to select the best clones. From the in *vitro* cell binding assay (Figure 1), two phage clones M6 and M13 bound melanoma and one clone M18 bound breast carcinoma cells with higher binding affinity and exhibited 8-40 fold increased signal strength compared to wide type phage. From the in *vivo* florescence imaging assay (Figure 2; Table 3) , three phage clones M4, M7, and M9 showed at least a two-fold increase in fluorescence signal strength post injection compared to pre-injection images performed on melanoma mouse models. Six clones M1, M2, M3, M6, M13 and M18 exhibited higher fluorescence signals in the breast carcinoma models.

We chose five selected peptide sequences M2, M6, M7, M13, M18 to be chemically synthesized, of which M2 and M7 represent clones were exclusively identified from in *vivo* assay. Based on the cell binding assay with these 5

peptides (Figure 4), 3 clones M7, M13 and M18 showed reduced cell absorption when competed with peptide complexes. The reduction indicated specific binding of the clones to either breast or melanoma cancer cells while M2 showed a slightly binding preference on melanoma cells. Some of the cells binding results are not consistent and the amount of the cell absorption of the radiolabelled peptide complexes increased when the non-radioactive peptides complexes were added on non-cancer human cell lines. The clone M2 had about ten folds increase when competed on melanocyte and human epithelial cell lines. The clones M7 and M13 showed about one fold increase on melanocyte and human epithelial cell lines, respectively. This could attribute to the aggregation of the peptides caused by additional excess peptides. In M7 and M13, the cysteins might form inter-molecular disulfide bonds to promote the aggregation. Other possible reasons may include the formation of multimers at the binding site stimulated by the excess amount of peptides.

The inclusion of the animal fluorescence study in *vivo* did help predict the best peptides: 1. It confirmed that M18 was a potentially good probe worth further investigation 2. The exclusive clone identified from *in vivo* fluorescence imaging assay with high fluorescence signals, M7, turned out to be a high binding capacity peptide. However, we saw that the phage clones M6, M13 had higher signals in the cell binding assay on melanoma cells but high fluorescence signals in vivo on breast cancer cells. In the peptide cell binding assays, M6 and M13 showed no dramatically difference on the two cancer cell lines. The same dicotomy existed with M7 when comparing the peptide cell binding assay to the in vivo

fluorescence animal study. It is still questionable whether M7, M6 and M13 can be used to image tumors.

On the phage particles, there are about 100 copies of phage coat protein pVIII fused with peptides, which means 100 copies of peptides are immobilized on one phage particle. This actually increases the local concentration of peptide compared to the synthetic free peptide in solution. When the peptides interact with the cell surface, the nearby coat proteins can influence the confirmation of the peptides or cell surface which may benefit the binding. So the peptides on the viron surfaces take advantage of phage for binding. Thus, the properties of peptides can be different from the phage clones bearing the peptides.

On the other hand, only one mouse was used for each peptide during the in vivo assay, this cannot generate a statistically significant conclusion. Though we removed the hair in the tumor area, the intrinsic fluorescence from the mice still affects the results. The way we analyzed the raw data may have generated some inaccuracy too considering the selection of the tumor area. So the in vivo fluorescent assay is not well developed and impossible to quantitate. However, the in *vivo* fluorescence screening step is a rapid assay to facilitate interrogating phage populations and it could be modified in the future to generate much more accurate data.

Through our selection, we were able to identify that peptide M13 had good potential as an imaging probe for melanoma, while the other two peptides M7 and M18 targeted breast carcinoma. However, these three peptides should be further tested in animal models to confirm their applications in cancer imaging.

REFERENCE

Bailey DL, Adamson KL. 2003. Nuclear medicine: from photons to physiology. Curr Pharm Des 9: 903-916.

Blok D, Feitsma RI, Vermeij P, Pauwels EJ. 1999. Peptide radiopharmaceuticals in nuclear medicine. Eur J Nucl Med 26: 1511-1519.

Boerman OC, Oyen WJ, Corstens FH. 2000. Radio-labeled receptor-binding peptides: a new class of radiopharmaceuticals. Semin Nucl Med 30: 195-208.

Bomanji JB, Costa DC, Ell PJ. 2001. Clinical role of positron emission tomography in oncology. Lancet Oncol 2: 157-164.

Fink AM, Holle-Robatsch S, Herzog N, Mirzaei S, Rappersberger K, Lilgenau N, Jurecka W, Steiner A. 2004. Positron emission tomography is not useful in detecting metastasis in the sentinel lymph node in patients with primary malignant melanoma stage I and II. Melanoma Res 14: 141-145.

Hodgson NC, Gulenchyn KY. 2008. Is there a role for positron emission tomography in breast cancer staging? J Clin Oncol 26: 712-720.

Kumar SR, Quinn TP, Deutscher SL. 2007. Evaluation of an 111In-radiolabeled peptide as a targeting and imaging agent for ErbB-2 receptor expressing breast carcinomas. Clin Cancer Res 13: 6070-6079.

Landon LA, Zou J, Deutscher SL. 2004. Is phage display technology on target for developing peptide-based cancer drugs? Curr Drug Discov Technol 1: 113-132.

Miao Y, Whitener D, Feng W, Owen NK, Chen J, Quinn TP. 2003. Evaluation of the human melanoma targeting properties of radiolabeled alpha-melanocyte stimulating hormone peptide analogues. Bioconjug Chem 14: 1177-1184.

Okarvi SM. 1999. Recent developments in 99Tcm-labelled peptide-based radiopharmaceuticals: an overview. Nucl Med Commun 20: 1093-1112.

Pasqualini R, Ruoslahti E. 1996. Organ targeting in vivo using phage display peptide libraries. Nature 380: 364-366.

Sawyer TK, Staples DJ, Castrucci AM, Hadley ME, al-Obeidi FA, Cody WL, Hruby VJ. 1990. Alpha-melanocyte stimulating hormone message and inhibitory sequences: comparative structure-activity studies on melanocytes. Peptides 11: 351-357.

Siegrist W, Solca F, Stutz S, Giuffre L, Carrel S, Girard J, Eberle AN. 1989. Characterization of receptors for alpha-melanocyte-stimulating hormone on human melanoma cells. Cancer Res 49: 6352-6358.

Smith GP. 1985. Filamentous fusion phage: novel expression vectors that display cloned antigens on the virion surface. Science 228: 1315-1317.

Timar J, Meszaros L, Ladanyi A, Puskas LG, Raso E. 2006. Melanoma genomics reveals signatures of sensitivity to bio- and targeted therapies. Cell Immunol 244: 154-157.

Van de Wiele C, De Vos F, Slegers G, Van Belle S, Dierckx RA. 2000. Radiolabeled estradiol derivatives to predict response to hormonal treatment in breast cancer: a review. Eur J Nucl Med 27: 1421-1433.

van der Flier A, Sonnenberg A. 2001. Function and interactions of integrins. Cell Tissue Res 305: 285-298.

van Dongen GA, Visser GW, Lub-de Hooge MN, de Vries EG, Perk LR. 2007. Immuno-PET: a navigator in monoclonal antibody development and applications. Oncologist 12: 1379-1389.

Wagner JD, Schauwecker D, Davidson D, Logan T, Coleman JJ, 3rd, Hutchins G, Love C, Wenck S, Daggy J. 2005. Inefficacy of F-18 fluorodeoxy-D-glucose-positron emission tomography scans for initial evaluation in early-stage cutaneous melanoma. Cancer 104: 570-579.

Widakowich C, de Castro G, Jr., de Azambuja E, Dinh P, Awada A. 2007. Review: side effects of approved molecular targeted therapies in solid cancers. Oncologist 12: 1443-1455.

Yu J, Smith GP. 1996. Affinity maturation of phage-displayed peptide ligands. Methods Enzymol 267: 3-27.

Chapter 3 A Generalized Kinetic Model for Amine Modification of Proteins with Application to Phage Display

This chapter is from the following paper:

Jin, X., Newton, J.R., Montgomery-Smith, S., Smith, G. P. (2009). A generalized kinetic model for amine modification of proteins with application to phage display. *BioTechniques*, 46, 175-182.

I am responsible for part of the experiments and initiated the manuscript.

Chapter 3 A Generalized Kinetic Model for Amine Modification of Proteins with Application to Phage Display

INTRODUCTION

Filamentous phage of the Ff class (derivatives of natural strains fd, f1 and M13) are the most common vectors in phage display technology (Smith *et al*., 1997). Library phage contain a foreign peptide or protein domain fused genetically to one of the phage coat proteins: in most cases, either to 1 to 5 copies of the minor coat protein pIII, or to 1 to ~150 copies of the major coat protein pVIII. The foreign protein or domain is thereby displayed on the outer surface of the virion, where it is accessible to antibodies, receptors or other solutes in the medium. Random peptide libraries (RPLs)—large populations of virions collectively displaying millions or billions of random peptides—are a rich source of high-affinity peptide ligands for a great diversity of target biomolecules. Such ligands can be specifically affinity-selected from the RPL by using the target biomolecule as an immobilized selector. Analogously, specific peptide ligands for target cells such as cancer cells, or for defined tissues in vivo such as tumors, can be affinity-selected using intact cells (Goodson *et al*.,1994)) or tissues in

Figure 1. Space-filling model (including hydrogens) of a short section of the tubular sheath of filamentous bacteriophage fd (Protein Data Bank accession 2C0X; refs. 4 and 5), with amino groups highlighted in black. The section depicted includes all or parts of 30 pVIII subunits (out of 2700 for wild-type virions, 4000 or more for some phage-display constructs), each with a highly exposed ε-amino group on the lysine at position 8 and a mostly buried α-amino group on the N-terminal alanine; only some of the α-amino groups are partly visible in the image. The overall diameter of the sheath is ~6 nm.

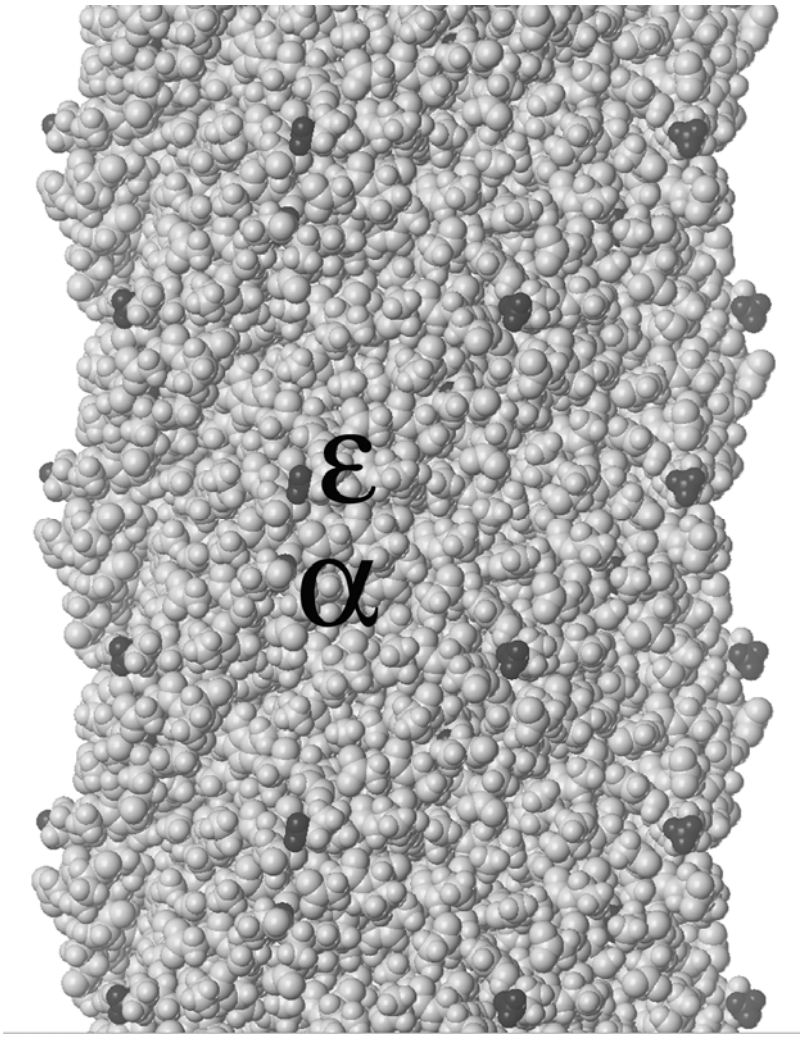
ε
α

living animals (Pasqualini *et al*., 1996) as selectors.

As shown in Figure 1, the filamentous virion has thousands of surface-exposed ε-amino groups—one on each subunit of the major coat protein pVIII (Marvin *et al*., 2006; Straus *et al*., 2008)—to which small chemical groups may be coupled without impairing structural integrity or infectivity (Armstrong *et al*.,1983). The α-amino groups on the pVIII subunits, though mostly buried in the structural model in Figure 1 and unreactive with acetimidate at pH 10 (Armstrong *et al*., 1983), may be reactive with amine-reactive reagents other than acetimidate. The ability to modify surface amines can be exploited in many research contexts. For instance, virions bearing tumor-avid peptides can be lightly modified with biotin and used to image tumors in vivo by a two-step "pretargeting" regimen (Newton *et al*., 2007). In the first step, tumor-bearing mice are injected with the biotinylated virions. In the second step, initiated only after non-tumor-bound virions have been allowed to clear, the mice are injected with ^{111}In-labeled streptavidin. The labeled streptavidin binds tightly to the tumor-targeted biotinylated virions, allowing the tumor to be imaged by single-photon emission computed tomography. Similarly, virions bearing tumor-avid peptides and lightly modified with near-infrared (NIR) fluorophors can be used to image tumors optically in *vivo* (Newton *et al*., 2006).

Success in such experiments requires that the exposed amines be modified to a sufficient level for the purpose at hand while avoiding the ill effects of over-modification, including detrimentally changing the virion's physical properties or sterically hindering specific binding by its displayed peptides. The effect of

modification level is well illustrated with biotinylated virions. Figure 2 shows a saturation curve for a streptavidin conjugate binding to virions biotinylated to various levels. According to that curve, virions reach half their maximum binding capacity at a modification level of about 0.03 biotins per pVIII subunit. That number would be an appropriate target modification level for almost all applications.

How can a desired target modification level be reliably achieved without a laborious series of pilot modifications? In this article, building on previous work (Smith, 2006), we develop a generalized kinetic model for protein amine modification that uses the results of test reactions at a few protein and reagent concentrations to calculate the expected results of similar modification reactions over a vast continuum of other protein and reagent concentrations. Modifications of filamentous phage pVIII with biotin and the NIR fluorophor Alexa Fluor 680 (AF680) serve as exemplars, but the model is applicable to any protein and amine-modifying reagent.

Figure 2. Saturation curve for binding of a streptavidin conjugate to biotinylated virions. Virions biotinylated to various levels were mixed with non-biotinylated virions at ratios ranging from 1:242 to 1:59048 in TBS, and 100-µl volumes containing a total of 2×10^{11} virions were adsorbed overnight at 4ºC to wells of a polystyrene 96-well ELISA dish. In these circumstances, the relative number of biotinylated virions immobilized per well will be proportional to the ratio of biotinylated to total virions, regardless of biotinylation level; those relative numbers are given in the figure. Wells were washed, reacted for 30 min at room temperature with 100 µl of an alkaline phosphatase-streptavidin conjugate (Catalog number 016-050-084, Jackson ImmunoResearch, West Grove, PA, USA) at 200 ng/ml in TBS/Tween (TBS supplemented with 0.5% Tween 20), washed, and developed and analyzed on a plate reader as described (12). Data were fitted to theoretical saturation curves of the form

$$Signal = \frac{S_{\max}}{1 + \left(\frac{m_{1/2}}{m} \right)^n},$$

where the independent variable = m = modification level (biotins per pVIII subunit); the adjustable curve shape parameters were $m_{1/2}$ (modification level resulting in half-maximal ELISA signal) and n (arbitrary positive exponent determining steepness of the curve); and the adjustable scale parameter = $S_{\max}$ (estimated maximal ELISA signal). The two shape parameters were constrained to be identical for all six data series (corresponding to the six relative numbers of immobilized biotinylated virions). Each data series was then normalized relative to a maximal theoretical ELISA signal $S_{\max}$ of 100, all six best-fit theoretical

saturation curves thereby becoming identical; that normalized best-fit theoretical saturation curve is the solid line in the graph. All the normalized data fit fairly well to this theoretical saturation curve, implying that the curve mainly reflects the binding capacity of individual virions, not the binding capacity of entire ELISA wells.

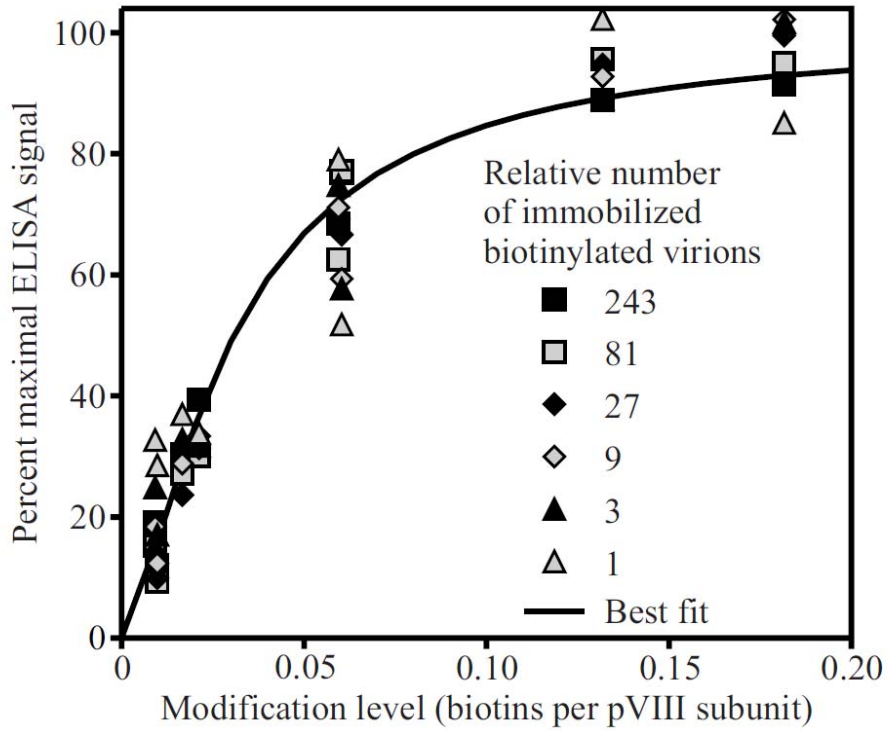
Percent maximal ELISA signal
100
80
60
40
20
0
0
0.05
0.10
0.15
0.20
Modification level (biotins per pVIII subunit)
Relative number
of immobilized
biotinylated virions
243
81
27
9
3
1
Best fit

MATERIALS AND METHODS

Modification procedure

Two N-hydroxysuccinimide (NHS) esters were chosen as amine-reactive reagents: the biotinylating reagent NHS-PEO_4-biotin (Catalog number 21329, Pierce Chemical Co., Rockford, IL, USA), and the NIR fluorophor labeling reagent sulfo-NHS-AF680 (Catalog number A20008, Invitrogen Corp., Carlsbad, CA). The reagents were dissolved just before use in dimethylsulfoxide (DMSO) to a range of concentrations (up to 17.4 mM sulfo-NHS-AF680; up to 34 mM NHS-PEO_4-biotin).

To 1.33×10^{13} fd virions (equivalent to 59.7 nmol pVIII subunits) diluted to various concentrations in CMF (136.9 mM NaCl, 2.68 mM KCl, 8.1 mM Na_2HPO_4, 1.47 mM KH_2PO_4, pH adjusted to 7.2 with HCl or NaOH) was added 1/9 volume of 1 M NaH_2PO_4, pH adjusted to 7.00 with NaOH, and up to 1/50 volume of reagent in DMSO; the vessels were vortexed immediately. Reactions were allowed to continue overnight (~12–18 hr) at room temperature in the dark; in view of the high reactivity of NHS esters, this was deemed more than enough time for the reactions to go to completion.

Removal of uncoupled biotin and AF680 and quantitation of modification level

The biotinylation reactions were diluted to 3 ml with TBS (150 mM NaCl, 50 mM Tris, pH adjusted to 7.5 with HCl), dialyzed against three changes of TBS in Slide-A-Lyzer cassettes with a nominal molecular weight cutoff of 10 kDa

(Catalog number 66380, Pierce Chemical Co., Rockford, IL), concentrated to ~50 µl by centrifugation through Centricon ultrafiltration devices with a nominal molecular weight cutoff of 100 kDa (Catalog number 4213, Millipore Corporation, Billerica, MA; no longer available; an essentially equivalent substitute is the Vivaspin 2 centrifugal concentrator, Catalog number VS0241 or VS0242, Sartorius Stedim Biotech, Goettingen, Germany), and diluted with 100 µl TBS. Dialysis was found to remove only ~94 percent of the uncoupled biotin, but ultrafiltration removed essentially all the rest. Virions were quantified by scanning suitable dilutions spectrophotometrically from 220 to 320 nm (Smith *et al*., 1993). Their content of coupled biotin was quantified as described (Smith, 2006) by proteinase K digestion (to cleave coupled biotin from the phage), centrifugation through Centricon ultrafiltration devices with a nominal molecular weight cutoff of 10 kDa to separate free biotin in the filtrate from phage and proteinase K in the retentate, and duplicate competition ELISA with the filtrates.

Reactions with sulfo-NHS-AF680 were diluted to 1 ml with CMF and the virions freed of uncoupled AF680 by three successive precipitations with polyethylene glycol (Yu *et al*., 1996) and two cycles of concentration from 1.8 ml to ~50 µl by centrifugation through Centricon ultrafiltration devices with a nominal molecular weight cutoff of 100 kDa as described above. (Dialysis was ineffective for this purpose, removing only about 60% of the uncoupled dye.) No AF680 was detectable spectrophotometrically in the final Centricon filtrate, indicating that uncoupled fluorophor had been completely removed. Suitable dilutions of the virions were scanned spectrophotometrically from 220 to 320 nm

and from 630 to 730 nm. AF680 content was calculated assuming a molar extinction coefficient of 184,000 at 679 nm; virion content was calculated from absorbance at 269 nm (Smith *et al.*, 1993) after subtracting 9.52 percent of the absorbance at 679 nm to correct for UV absorbance by AF680.

RESULTS AND DISCUSSIONS

The assumed pathways for irreversible modification of amines and consumption of amine-reactive reagent by hydrolysis are diagrammed in Figure 3. The protein molecule is treated as a collection of independently reacting amines, each corresponding to a particular amino group (α or ε) at a particular site in the protein structure. The top arrow represents the desired reaction, in which protein amines are modified by reaction with the reagent. Unlike the single-amine kinetic model published earlier (Smith, 2006), the generalized model presented here accommodates multiple amino groups reacting with the reagent with different second-order rate constants k_i (μM^{-1} sec^{-1}). It will be convenient in what follows to index those amines in order of reactivity ($k_{i+1} \leq k_i$); this indexing convention ensures that k_1, the largest rate constant, is greater than zero (assuming modification is possible at all). If there is a set of amino groups in the protein molecule that can be assumed to be kinetically equivalent (react with the same second-order rate constant), they can be bundled together and treated as a single amine j with a copy number M_j equal to the number of individual amines in the bundle; the copy number for an individual unbundled amine is 1. Competing with amine modification, and represented by the bottom arrow in Figure 3, is hydrolysis of reagent to its unreactive hydrolyzed form. As before (Smith, 2006), hydrolysis is assumed to proceed in two independent, additive ways: by a protein-independent pathway with a first-order rate constant k_h (sec^{-1}); and by a protein-

Figure 3. Reaction scheme for modification of amines and consumption of reagent by hydrolysis. The symbols above and below the arrows are the rate constants for the pathways (see text).

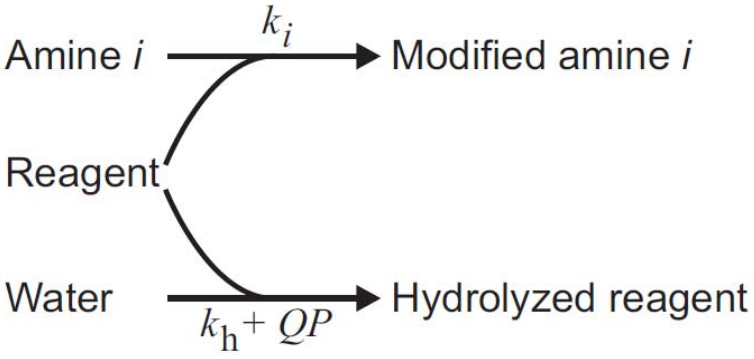
Amine i
k_i
Modified amine i
Reagent
Water
$k_h + QP$
Hydrolyzed reagent

mediated pathway at a rate that is proportional to the protein concentration P (μM) with a second-order rate constant Q (μM^{-1} sec^{-1}). As a catalyst of hydrolysis, the protein is presumed to remain at the same effective concentration P throughout the reaction despite its growing amine modification level. The state of the system at completion of the reaction, when all reagent is consumed, can depend only on the timeless ratios of the rate constants, reducing the number of independent kinetic parameters to $N + 1$, where N is the number of amines or amine bundles; we have chosen the ratios k_h/k_1 (μM), Q/k_1 (dimensionless) and k_i/k_1 (dimensionless; $i = 2, 3,\ldots, N$). Since k_1 is greater than 0 according to the indexing convention above, all these ratios exist, though some may be 0. Under the foregoing assumptions, the modification level m (number of modified amines per protein molecule) at completion of the reaction of protein at concentration P with reagent at initial concentration R (μM) is given by

$$m = \frac{R - \left(\frac{k_h}{k_1} + \frac{Q}{k_1}P\right)\lambda}{P}, \text{ where } \lambda \text{ is the root of the function}$$
$$f(\lambda) = R - \left(\frac{k_h}{k_1} + \frac{Q}{k_1}P\right)\lambda - P\sum_{i=1}^{N} M_i\left(1 - \exp\left(-\frac{k_i}{k_1}\lambda\right)\right) \qquad \text{Eq. 1}$$

The derivation of Equation 1 and guidance for computing the root λ by the Newton-Raphson method are given in the document in Supplementary Material.

The foregoing generalized kinetic model does not specify the values of the kinetic parameters in Equation 1. Those parameter values must instead be determined empirically for each protein reacting with each reagent under given reaction conditions (buffer and temperature). To that end, a series of test

reactions is carried out in which the protein at a range of concentrations P is reacted with reagent at a range of initial concentrations R under the given reaction conditions, the resulting final modification level m being measured in each case. The values of the kinetic parameters are then adjusted so as to optimize the overall agreement between the theoretical modification levels calculated from Equation 1 and the modification levels actually observed in the test series. Once optimal parameter values have been determined, the results of the test series reactions can be extrapolated to reactions at quite different protein and initial reagent concentrations. Most frequently, the user will want to know the initial reagent concentration R required to achieve a given target modification level m when the protein concentration is P. Rearranging Equation 1, that required initial reagent concentration R can be calculated as

$$R = mP + \left(\frac{k_h}{k_1} + \frac{Q}{k_1} P \right) \lambda, \text{where } \lambda \text{ is the root of the function}$$
$$f(\lambda) = m - \sum_{i=1}^{N} M_i \left(1 - \exp\left(-\frac{k_i}{k_1} \lambda \right) \right) \qquad \text{Eq. 2}$$

In the case of filamentous virions, the effective protein concentration P is the total concentration of pVIII subunits—bearers of more than 98 percent of the virion's accessible amines. There are two amines per subunit, each with a copy number of 1. No assumption is (or need be) made about which amine is more reactive; thus whether amine 1 is the α or ε amino group remains unspecified.

Results of test modification reactions with NHS-PEO_4-biotin and sulfo-NHS-AF680 are shown in panels A and B of Figure 4, respectively (an exemplar spreadsheet for the analysis in panel A is included in Supplementary Material).

The solid lines are isomodification contours predicted by Equation 2 for the optimized values of the adjustable parameters given in Table 1. Each contour corresponds to a particular modification level *m*; each point on the contour gives a combination of pVIII and initial reagent concentrations predicted to yield that modification level. Superimposed on the contours are the test reaction data on which the optimized parameter values are based. For each test reaction, the gray circle marks the actual concentrations of pVIII and reagent, while the horizontal bars plot the initial reagent concentration *R* that according to Equation 2 with the optimized parameter values would theoretically be required achieve the modification level actually measured for that reaction (one bar for each of the duplicate determinations of biotinylation level in panel A).

The closeness of the horizontal bars to each other in panel A testifies to the excellent reproducibility of the duplicate biotin determinations; the closeness of those bars to their corresponding gray circles testifies to the excellent fit of the observed data to the theoretical calculations over a wide range of pVIII concentrations. Independent IgG test reactions with different tubes of pre-weighed biotinylating reagent from the same batch gave entirely consistent results (Smith, 2006), and batch-to-batch consistency is also good (data not shown). Using the optimized parameter values in Table 1, therefore, Equation 2 provides a reliable way to calculate the concentration of NHS-PEO_4-biotin required to biotinylate virions to any chosen target level under the conditions of our test reactions.

Figure 4. Modification of fd virions with NHS–PEO_4-biotin (A) and sulfo-NHS-AF680 (B). The solid lines are isomodification contours predicted by Eq. 2 for the optimized values of the adjustable parameters given in Table 1. The open circles and horizontal bars represent the test reaction data used to optimize those parameter values, as explained in the text.

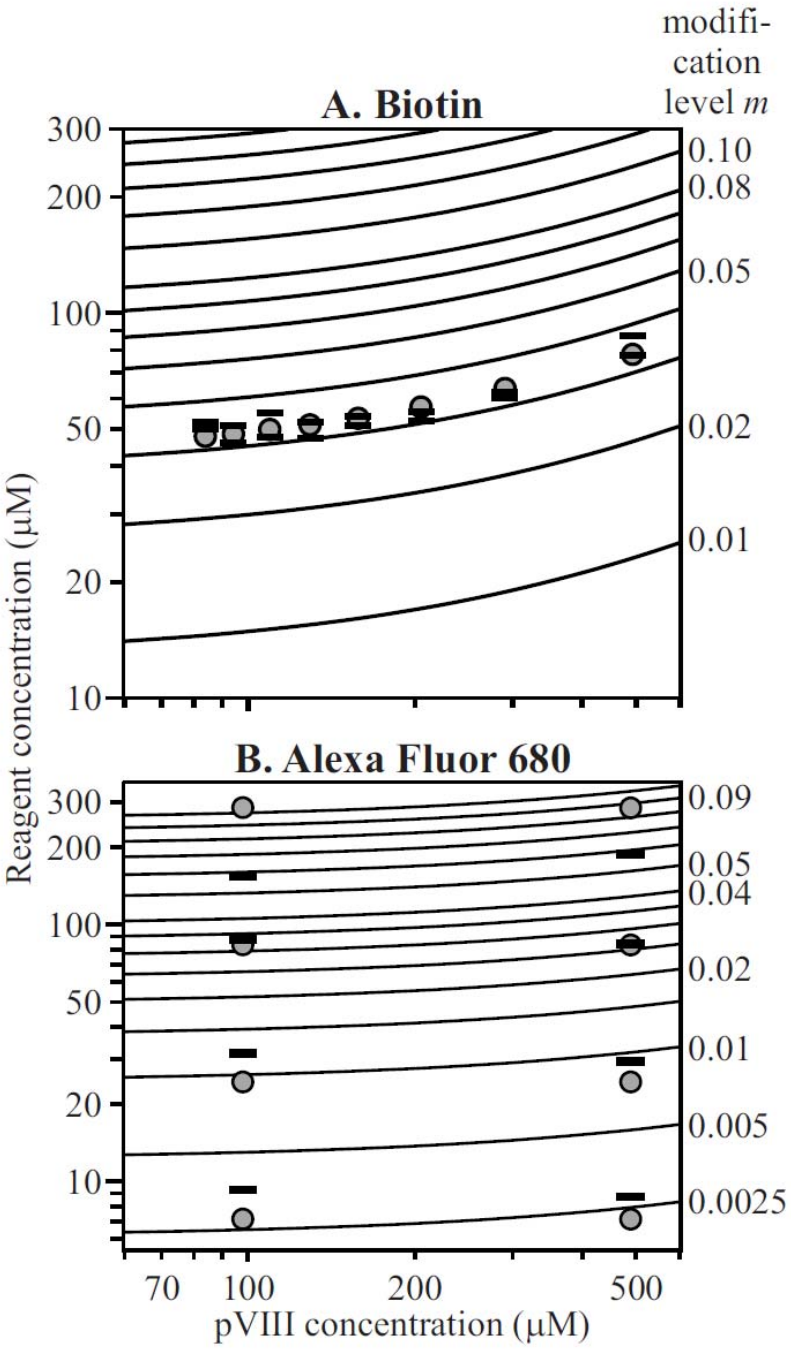
modifi-
cation
level m
A. Biotin
300
200
100
50
20
10
0.10
0.08
0.05
0.02
0.01
B. Alexa Fluor 680
300
200
100
50
20
10
0.09
0.05
0.04
0.02
0.01
0.005
0.0025
Reagent concentration (μM)
70
100
200
500
pVIII concentration (μM)

Table 1. Optimized parameter values for phage pVIII modification reactions. The kinetic parameters in the last three columns were adjusted so as to minimize the overall deviation of the observed modification levels for the test reactions at various protein and initial reagent concentrations from the corresponding theoretical modification levels calculated with Equation 1 for those same protein and initial reagent concentrations. The metric for overall deviation was the sum of the squares of the logarithms of the ratios of observed to theoretical modification levels.

Reagent	Q/k_1	k_h/k_1 (μM)	k_2/k_1
NHS-PEO_4-biotin	1.080	1274.1	0
sulfo-NHS-AF680	0.4717	2445.7	0

The agreement between theory and data is reasonably close in panel B, though not as close as in panel A. The reliability of theoretical predictions for modification with the sulfo-NHS-AF680 reagent is not as well established as for biotinylation with NHS-PEO_4-biotin, since batch-to-batch consistency has not yet been assessed. In using Equation 1 or 2 in conjunction with the optimized sulfo-NHS-AF680 parameter values in Table 1, therefore, the possibility of some deviation from expectation should be anticipated.

According to Equation 1 with the optimized phage biotinylation parameters in Table 1, the molar ratio of reagent to pVIII subunits required to biotinylate 60 μM pVIII to a level of 0.03 biotins per pVIII subunits is 0.71. If that same molar ratio is used to biotinylate 600 μM pVIII, the expected level is 0.158—more than 5 times higher. In general, the molar ratio of modifying reagent to target protein is a wholly inadequate description of reaction conditions for amine modifications; both protein and reagent concentrations must be specified individually (Smith, 2006). On the other hand, the concentration of reagent required to achieve a biotinylation level of 0.03 rises only 6.3 percent (from 39.4 to 42.0 μM) as the pVIII subunit concentration increases 5 fold from 10 to 50 μM. In general, the isomodification contours flatten out at the lowest target protein concentrations, as is evident in Figure 4. That flattening implies that a given reagent concentration will result in the same modification level for a wide range of target protein concentrations, as long as all those concentrations are sufficiently low (Smith, 2006).

For both phage modifications reported in Table 1, the optimized value of k_2/k_1 turned out to be 0, implying that the original single-amine kinetic model (Smith, 2006) fits the data just as well as the generalized multi-amine model presented here. This is not significant evidence that there is only one reactive amine per pVIII subunit, however. Indeed, even if k_2/k_1 is constrained to be 1 (i.e., if both α and ε amino groups are assumed to be equally reactive), adjustment of the other two parameters allows the predictions of Equation 1 to fit the observed modification levels nearly exactly as well as for the optimized parameter values, and makes discernible changes only in the highest isomodification contours. The advantage of the generalized multi-amine kinetic model over the original single-amine model will therefore only be fully realized for test reactions covering a much broader range of reagent concentrations than were interrogated in the exemplars reported here.

REFERENCES

Armstrong J, Hewitt JA, Perham RN. 1983. Chemical modification of the coat protein in bacteriophage fd and orientation of the virion during assembly and disassembly. EMBO J 2: 1641-1646.

Day LA. 1969. Conformations of single-stranded DNA and coat protein in fd bacteriophage as revealed by ultraviolet absorption spectroscopy. J Mol Biol 39: 265-277.

Goodson RJ, Doyle MV, Kaufman SE, Rosenberg S. 1994. High-affinity urokinase receptor antagonists identified with bacteriophage peptide display. Proc Natl Acad Sci U S A 91: 7129-7133.

Marvin DA, Welsh LC, Symmons MF, Scott WR, Straus SK. 2006. Molecular structure of fd (f1, M13) filamentous bacteriophage refined with respect to X-ray fibre diffraction and solid-state NMR data supports specific models of phage assembly at the bacterial membrane. J Mol Biol 355: 294-309.

Newton JR, Kelly KA, Mahmood U, Weissleder R, Deutscher SL. 2006. In vivo selection of phage for the optical imaging of PC-3 human prostate carcinoma in mice. Neoplasia 8: 772-780.

Newton JR, Miao Y, Deutscher SL, Quinn TP. 2007. Melanoma imaging with pretargeted bivalent bacteriophage. J Nucl Med 48: 429-436.

Pasqualini R, Ruoslahti E. 1996. Organ targeting in vivo using phage display peptide libraries. Nature 380: 364-366.

Smith GP, Scott JK. 1993. Libraries of peptides and proteins displayed on filamentous phage. Methods Enzymol 217: 228-257.

Smith GP, Petrenko VA. 1997. Phage Display. Chem Rev 97: 391-410.

Smith GP. 2006. Kinetics of amine modification of proteins. Bioconjug Chem 17: 501-506.

Straus SK, Scott WR, Symmons MF, Marvin DA. 2008. On the structures of filamentous bacteriophage Ff (fd, f1, M13). Eur Biophys J 37: 521-527.

Yu J, Smith GP. 1996. Affinity maturation of phage-displayed peptide ligands. Methods Enzymol 267: 3-27.